phys. stat. sol. (b) 133, 583 (1986)

Subject classification: 61.80 and 78.70; S1.1; S1.2; S5; S5.11; S5.12

Institute of Nuclear Physics, Academy of Sciences of the USSR, Novosibirsk[1])

Radiation Yield of High-Energy Electrons in Thick Crystals

By

V. N. Baier, V. M. Katkov, and V. M. Strakhovenko

1. Description of Radiation in Thick Crystals

According to the performed analysis [1, 2] dealing with the kinetics of the distribution, which is due to multiple scattering, the DF for large depths (l) is of the form

$$\begin{aligned} dF^{pl}(\boldsymbol{v}_\perp, x, l) &= \frac{dx\, d^2v_\perp}{d_{pl}\, \pi g(l)} \exp\left(-\frac{\boldsymbol{v}_\perp^2}{g(l)}\right) \\ dF^{ax}(\boldsymbol{v}_\perp, \boldsymbol{\varrho}, l) &= \frac{d^2\varrho\, d^2v_\perp}{S\, \pi g(l)} \exp\left(-\frac{\boldsymbol{v}_\perp^2}{g(l)}\right) \end{aligned} \tag{1}$$

where x, $y(\boldsymbol{\varrho})$ are the transverse coordinates: $|x| \leqq d_{pl}/2$ for the planar case and $|\boldsymbol{\varrho}| \leqq r_0$ for the axial case; $S = \pi r_0^2$ is the area of a cell in the transverse plane which contains the projection of one atomic chain, and $n_\perp = 1/S$ is the density of the chains of atoms (axes). The quantity $g(l)$ has the form

$$g(l) = \Delta^2 + \int_0^l \dot{\vartheta}_s^2(t)\, dt\,, \tag{2}$$

where $\dot{\vartheta}_s^2$ is the rate of variation of the squared angle of multiple scattering in an appropriate amorphous medium. The time (depth) dependence of $\dot{\vartheta}_s^2$ is connected with the variation of the particle energy because of radiation losses. The first term in $g(l)$ reflects the character of the angular (velocity) distribution established at the initial stage of electron motion in a crystal which depends on the angular (over ϑ_0) distribution in an incident beam. Even with the angle of incidence $\vartheta_0 = 0$, the angular spread of particles in the crystal proves to be roughly equal to the Lindhard angle: $\vartheta_c = \sqrt{2U_0/\varepsilon}$ (U_0 is the depth of the potential well and ε is the energy of a particle); therefore, assuming the incident beam to be rather narrow, $\vartheta_0 \leqq \vartheta_c$, we can put $\Delta^2 = c_1 \vartheta_c^2$, where c_1 is a coefficient of the order of unity. The magnitude of c_1 can be influenced also by the imperfectness

and modifications of incoherent contributions are small, distinctions in the soft cascade development in crystal and amorphous media are mainly due to the coherent contribution to the radiation. This contribution changes the shape of photon spectra, enriching their soft part and noticeably diminishing the effective radiation length L_{ef} determined by the relation

$$L_{ef}^{-1} = \tilde{L}_{rad}^{-1} + L_{ch}^{-1} .$$

So, for the $< 111 >$ axis of tungsten, we find $L_{ef} \simeq 0.13\,cm$ at $\varepsilon = 2GeV$ and $L_{ef} \simeq 0.08\,cm$ at $\varepsilon = 5GeV$, which are several times less than the amorphous value $L_{rad} \simeq 0.35\,cm$. Thus in a crystal the initial electron is converted into photons along appreciably shorter length than in a corresponding amorphous medium, while further development of the soft shower in both media is more or less the same. Hence the most pronounced distinctions of shower characteristics in the amorphous and crystal case appear for small thicknesses. It is clear that for the valuable use of crystal properties in the case of suggested target composed of crystal and amorphous layers, the former must be of a few L_{ef} thick.

tained within the approximation mentioned . We have compared the shape of the spectrum (2) with available experimental data, but this procedure is somewhat indirect for several reasons. Sometimes very thin samples were used where the distribution of electrons over transverse coordinates was far from being uniform, sometimes energy loss spectra were measured which are noticeably different from true intensity spectra, sometimes emitted photons were collimated that also results in a change of the observed shape of spectra. Nevertheless, a qualitative agreement of the spectrum (2) with known experimental data holds for all energies beginning with $900\,MeV$.

The contribution to any process going on in a crystal is a sum $Y = Y_{coh} + Y_{inc}$ where, generally speaking, the incoherent contribution Y_{inc} differs from the amorphous value Y_{am}. The scale of this modification depends on the process under consideration. For the total intensity of the incoherent radiation and the quantity $\tilde{L}_{rad} = \varepsilon / I_{br}$ connected to it, the typical scale of diminishing of I_{br} as compared to I_{am} at room temperature is depending on media 9 to 13 per cent. The diminishing of the total probability of pair-production is of the same order of magnitude. In particular, we obtain for tungsten in the case of a full screening $\tilde{L}_{rad} = 1.1\, L_{rad}$. As far as the coherent contribution to the pair-production probability is negligible in the considered energy region

given by eq.(2) with a corresponding expression obtained in CFA BKS(1987) for the uniform distribution over transverse coordinates. So eq.(2) reproduces the energy dependence of coherent contribution to the radiation length $L_{ch} = \varepsilon/I_{ch}(\varepsilon)$ inherent to CFA which as mentioned above is valid in a wide energy range. For the sake of possible use, we have fitted our results for the function $r(\varepsilon)$ in the energy interval $\varepsilon < 5GeV$ by a polynomial

$$r(\varepsilon) = \sum_{n=0}^{9} a_n \varepsilon^n ,$$

where ε is measured in GeV and coefficients a_n for $<110>$-axis of Si and Ge crystals and for $<111>$-axis of W crystal are calculated. The fitting provides the accuracy better than 1 percent for Si and Ge and better than 3 percent for W.

The position of a maximum in the spectrum given by eq.(2) is always consistent with the estimate (1). For relatively small energies when $\rho_c \ll 1$ and correspondingly $u_0 \ll 1$, we can neglect the first term in the right-hand side of eq.(3) since $\rho_c/\chi_s = 2ma_s \gg 1$. In this case the spectrum (2) has a maximum at $\omega = \omega_{max} \simeq 0.05\varepsilon u_0 \simeq 2\varepsilon\sqrt{\rho_c}/(ma_s)$ which evidently coincides in this (dipole) approximation with eq.(1). When $\rho_c \gg 1$ and CFA is valid the spectrum (2) reproduces not only the position of a maximum but also the shape of spectral distributions like those shown in Fig.2 of BKS(1987) ob-

where a_s is the screening radius of a corresponding potential and

$$\rho \simeq (2V_0/m\theta_0)^2 \; for \; \theta_0 > \theta_c$$

and

$$\rho \simeq \rho_c = 2V_0\varepsilon/m^2 \; for \; \theta_0 < \theta_c .$$

The estimate BKS(1987) for the characteristic frequency of emitted photons ω at given frequency of motion ω_0 reads

$$u \equiv \frac{\omega}{\varepsilon - \omega} \simeq \frac{2N\omega_0\varepsilon}{m^2\,(1 + \rho/2)}, \qquad (1)$$

where N is the characteristic number of emitted harmonics. Note that N = 1 for $\rho \leq 1$ and N $\propto \rho^{3/2}$ for $\rho \gg 1$. Using also that $\omega_0 \sim \theta_0/a_s$, we suggest to describe the radiation from channeled and moving not very high above the potential barrier particles the following heuristic intensity spectrum:

$$\frac{dI_{ch}}{d\omega} = \frac{r(\varepsilon)\varepsilon}{u_0(\varepsilon)}\left[1 + \frac{1}{(1+u)^2}\right]\left(\frac{u}{u_0}\right)^{1/3} \ln\left(\frac{u_0}{u}\right)\vartheta(u_0 - u), \qquad (2)$$

where $\vartheta(z) = 1$ for $z > 0$ and $\vartheta(z) = 0$ for $z < 0$,

$$u_0 = \frac{25}{6}\chi_s + 80\,\frac{1}{ma_s}\,\frac{\sqrt{\rho_c}}{(2 + \rho_c)}. \qquad (3)$$

The function $r(\varepsilon)$ in eq.(2) is determined by the condition of the coincidence of the total intensity

$$I_{ch}(\varepsilon) = \int_0^{\varepsilon} d\omega \left(\frac{dI_{ch}}{d\omega}\right)$$

BKS NIM B 103 (1995) 147

Here we consider axial alignment when θ_0 with respect to the chosen axis is not too large as compared to the critical (Lindhard) angle $\theta_c = (2V_0/\varepsilon)^{1/2}$,where V_0 is a typical scale of the corresponding potential and ε is the particle energy, since in this case the most pronounced effects take place.

Let us start with the coherent contribution to the radiation. As already mentioned, at sufficiently high energies corresponding expressions valid at any angle of incidence θ_0 were obtained in BKS(1987). For $\theta_0 \ll V_0/m$ they reproduce CFA-limit. But even if the initial electron energy is high enough to apply mentioned description, charged particles arising in the course of a shower development may not satisfy this condition. In the case of a soft cascade we have to describe the radiation from these "soft" particles as well. Let us remind that within semiclassical theory of the QED- processes in any external field there are only two parameters: ρ and χ. The parameter ρ is a measure of the particle velocity deviation from a straight line in units of the natural emission angle $\gamma^{-1} = m/\varepsilon$, while the parameter χ being the ratio of the external field strength in the particle rest system to the critical QED-value $E_c = 1.32 \cdot 10^{16}\, eV/cm$ is responsible for the magnitude of quantum recoil effects. In crystals

$$\chi \sim \chi_s = V_0\varepsilon/m^3 a_s ,$$

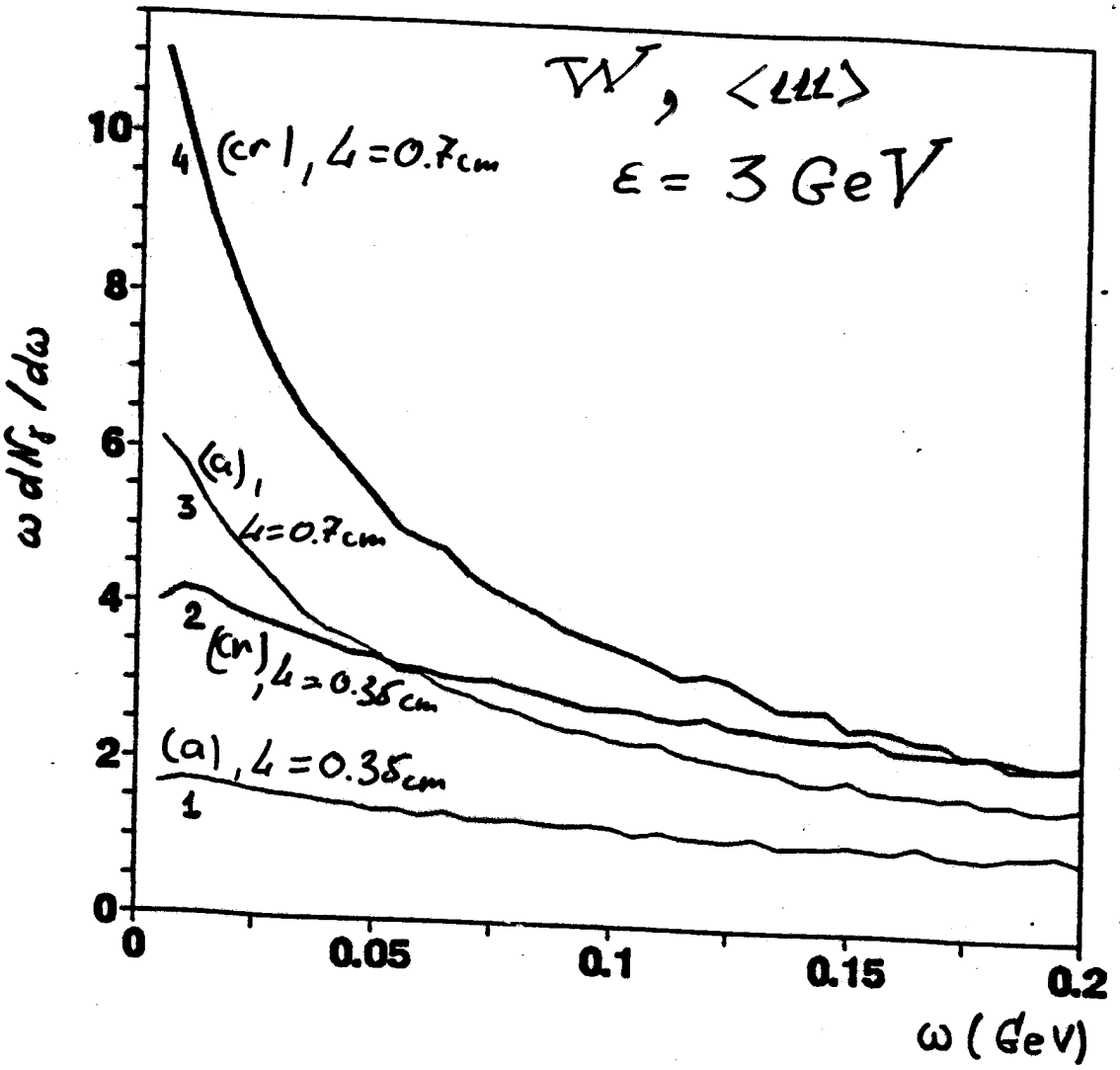
W, <111>
ε = 3 GeV
4 (cr), L = 0.7cm
3 (a), L = 0.7cm
2 (cr), L = 0.35cm
1 (a), L = 0.35cm
ω dN_γ / dω
ω (GeV)
0
2
4
6
8
10
0
0.05
0.1
0.15
0.2

Fig. 1(a)

esides the radiation under study, the bremsstrahlung (below with the subscript ') also contributes to the intensity. Generally speaking, the bremsstrahlung can ige in comparison with an amorphous medium, under channeling conditions. No oretical analysis of this problem is available. Nevertheless, to give an idea of the

Table 1

Parameters of the potential for the ⟨111⟩ axis and some characteristics of the radiation

al	u_1 (10^{-10} m) $T = 293$ K	V_0 (eV)	U_0 (eV)	β	a_s (10^{-10} m)	$c = \frac{L_{rad}}{L_{ph}}$	R	ω_{ch} (MeV)	L_0 (mm)
(d)	0.040	29	103	0.025	0.326	0.61	1.87	21.1	15.6
i	0.075	54	106	0.150	0.30	0.57	0.80	23.3	15.3
/	0.082	135	280	0.135	0.306	0.49	1.16	37.0	4.8
r	0.061	165	358	0.122	0.272	0.48	1.64	47.0	3.6
e	0.068	180	363	0.145	0.276	0.48	1.46	46.6	3.15
e	0.085	91	191	0.13	0.30	0.51	0.53	31.1	4.3
93 K)	0.050	417	937	0.115	0.215	0.50	1.48	96.2	0.65
K)	0.030	348	1255	0.027	0.228	0.50	2.38	105.0	0.61

plitude of thermal vibrations, V_0, β, a_s parameters of the potential (6), U_0 depth of the potential, c ratio of the radiation length to the effective length of photon absorption, $R = I_{as}/I_{br}$ ratio = 1 GeV, ω_{ch} frequency calculated by means of (16) at $\varepsilon_0 = 1$ GeV, L_0 optimal thickness of rystal at $\varepsilon_0 = 1$ GeV.

nitude of the effect, we shall make use of the model of a corresponding amorphous ium for a description of the bremsstrahlung. Assuming the condition (4) to be fied, for the bremsstrahlung intensity at depth l we find

$$\frac{dI_{br}}{d\Omega} = \frac{I_{br}}{\pi g(l)} \equiv \frac{1}{\pi g(l)} \frac{\varepsilon}{L_{rad}}. \tag{9}$$

[1, 2] the energy variation will be taken into account in an adiabatic approximawith due regard for both mechanisms of radiation losses. Hence, for the energy epth l we have

$$\frac{\varepsilon(s)}{\varepsilon_0} = \frac{e^{-s}}{1 + R(\varepsilon_0)(1 - e^{-s})} = G(s), \tag{10}$$

ere $s = l/L_{rad}$, ε_0 is the initial energy and $R(\varepsilon) = I_{as}/I_{br}$. Substituting $\varepsilon(s)$ into nd (9), we find

$$\frac{dI_{ch}}{d\Omega} = \frac{\alpha}{(2\pi)^2} \frac{\varepsilon_0^3 R(\varepsilon_0)}{m^2 L_{rad}} G^2(s) f(s),$$

$$\frac{dI_{br}}{d\Omega} = \frac{\alpha}{(2\pi)^2} \frac{\varepsilon_0^3}{m^2 L_{rad}} G(s) f(s), \tag{11}$$

re

$$f(s) = \left[\frac{1}{2}(1+R)^2(e^{2s}-1) - 2R(1+R)(e^s-1) + R^2 + \frac{l_a}{L_{rad}}\right]^{-1}, \tag{12}$$

$R \equiv R(\varepsilon_0)$, l_a is defined in (3), and $G(s)$ is given by (10).

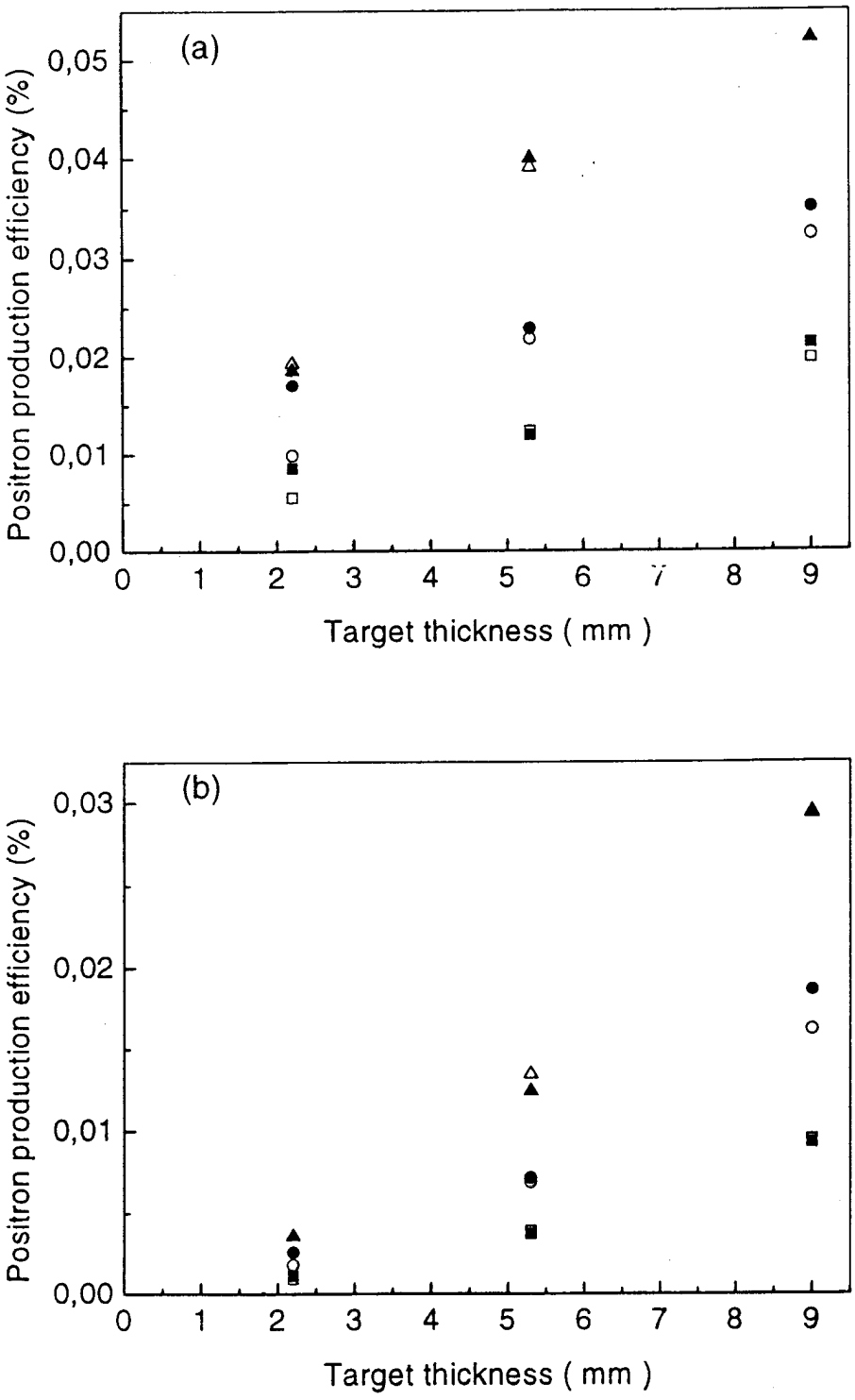

FIG. 6: Positron production efficiency from crystal (a) and amorphous (b) targets depending on thickness. Open symbols - our calculation, filled symbols - results from Fig.5 of [15]; $\triangle$ are for $p = 20$ Mev/c, $\bigcirc$ are for $p = 15$ Mev/c, and $\square$ are for $p = 10$ Mev/c.

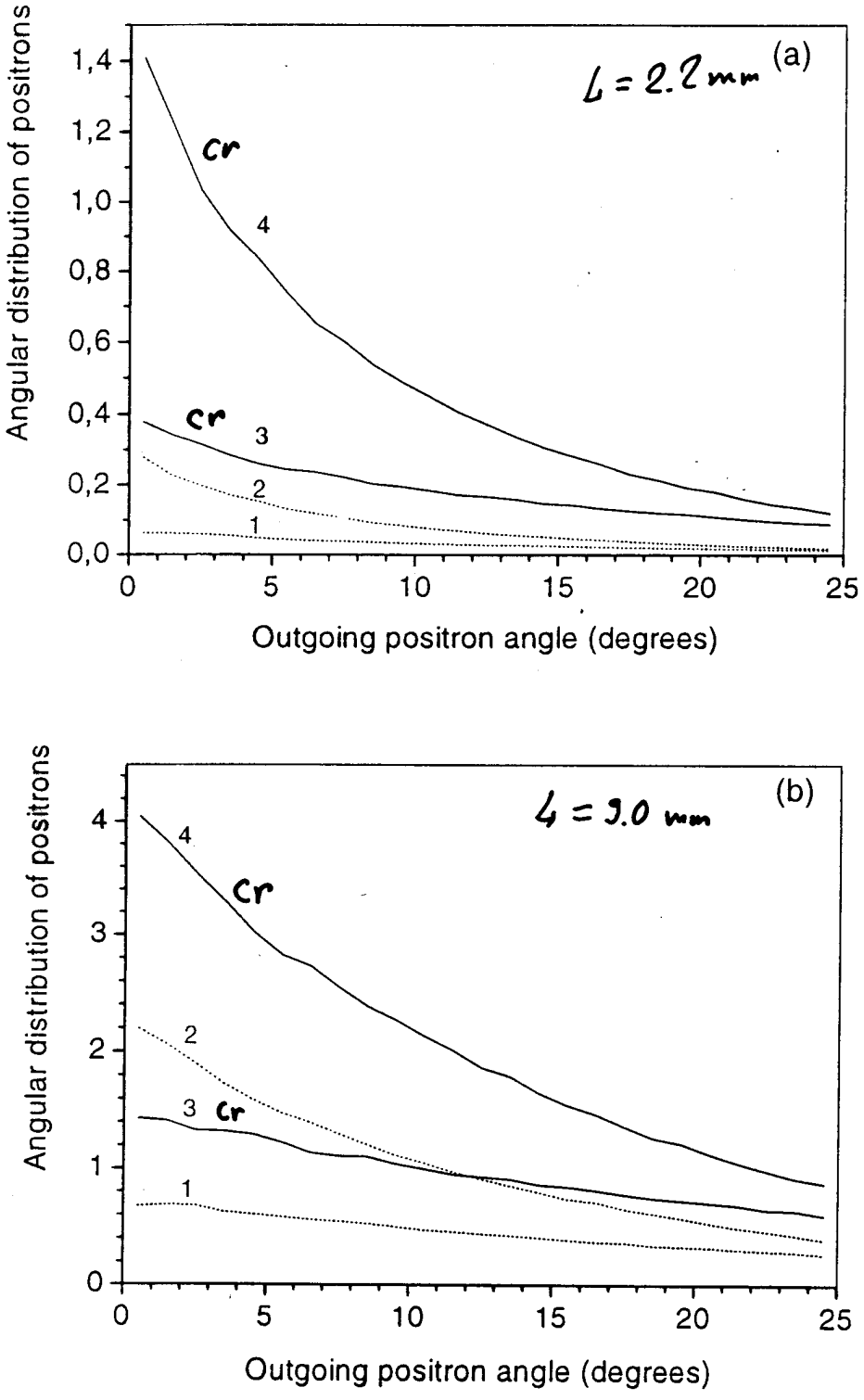

FIG. 5: Angular distribution $dN^{(+)}/d\Omega$ depending on outgoing positron angle at $L = 2.2$ mm (a) and at $L = 9.0$ mm (b) for $p_\perp \in (8.5 \div 11.5)$ Mev/c (curves 1 and 3) and for $p_\perp \in (17 \div 23)$ Mev/c (curves 2 and 4). Solid curves represent the yield from crystal and dotted from amorphous targets.

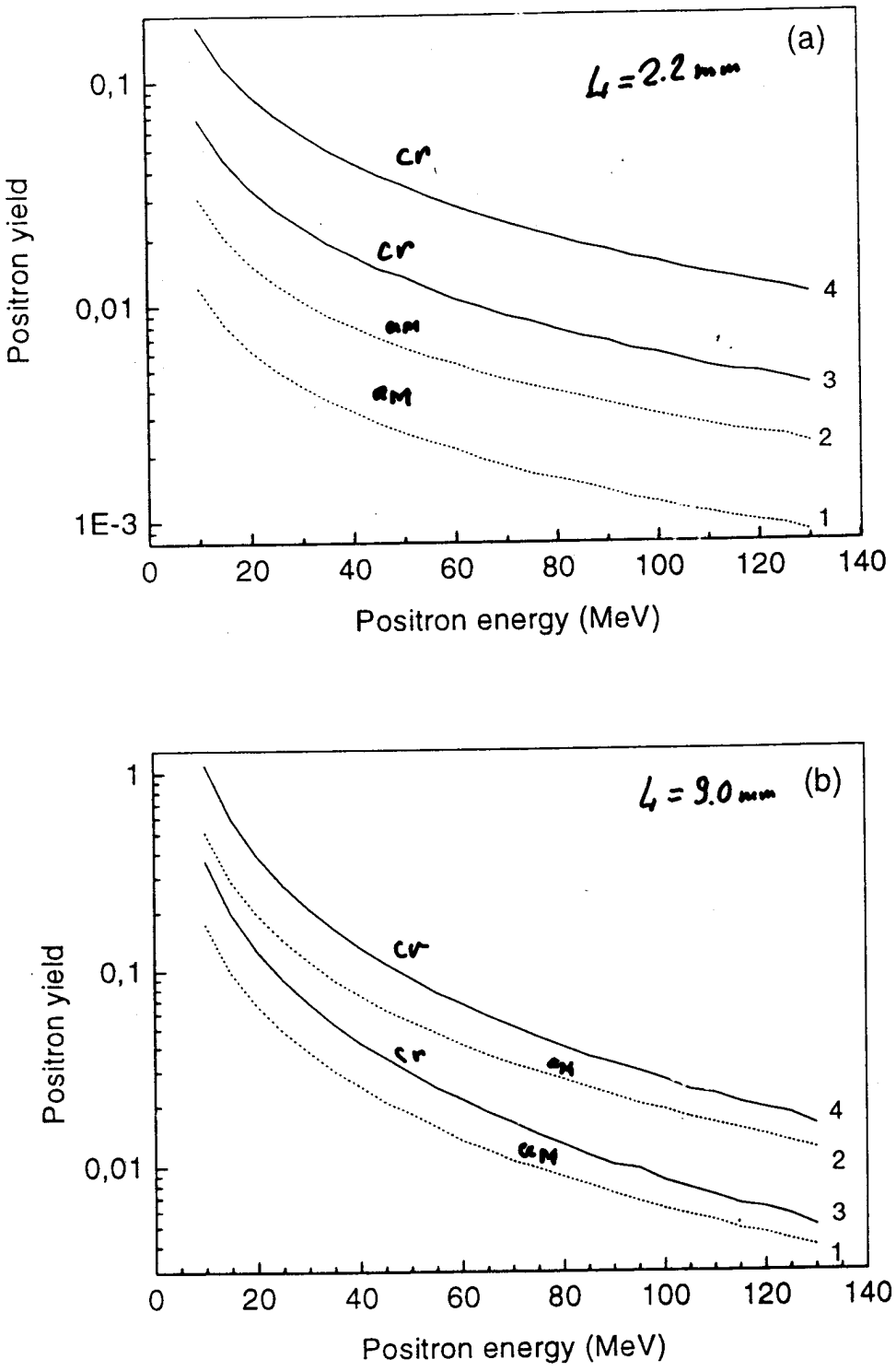

FIG. 4: Positron yield depending on energy at $L = 2.2$ mm (a) and $L = 9.0$ mm (b) for $p_{\perp}^{max} =$ 2.5 MeV/c (curves 1 and 3) and for $p_{\perp}^{max} = 5$ MeV/c (curves 2 and 4). Solid curves represent the yield from crystal and dotted from amorphous targets.

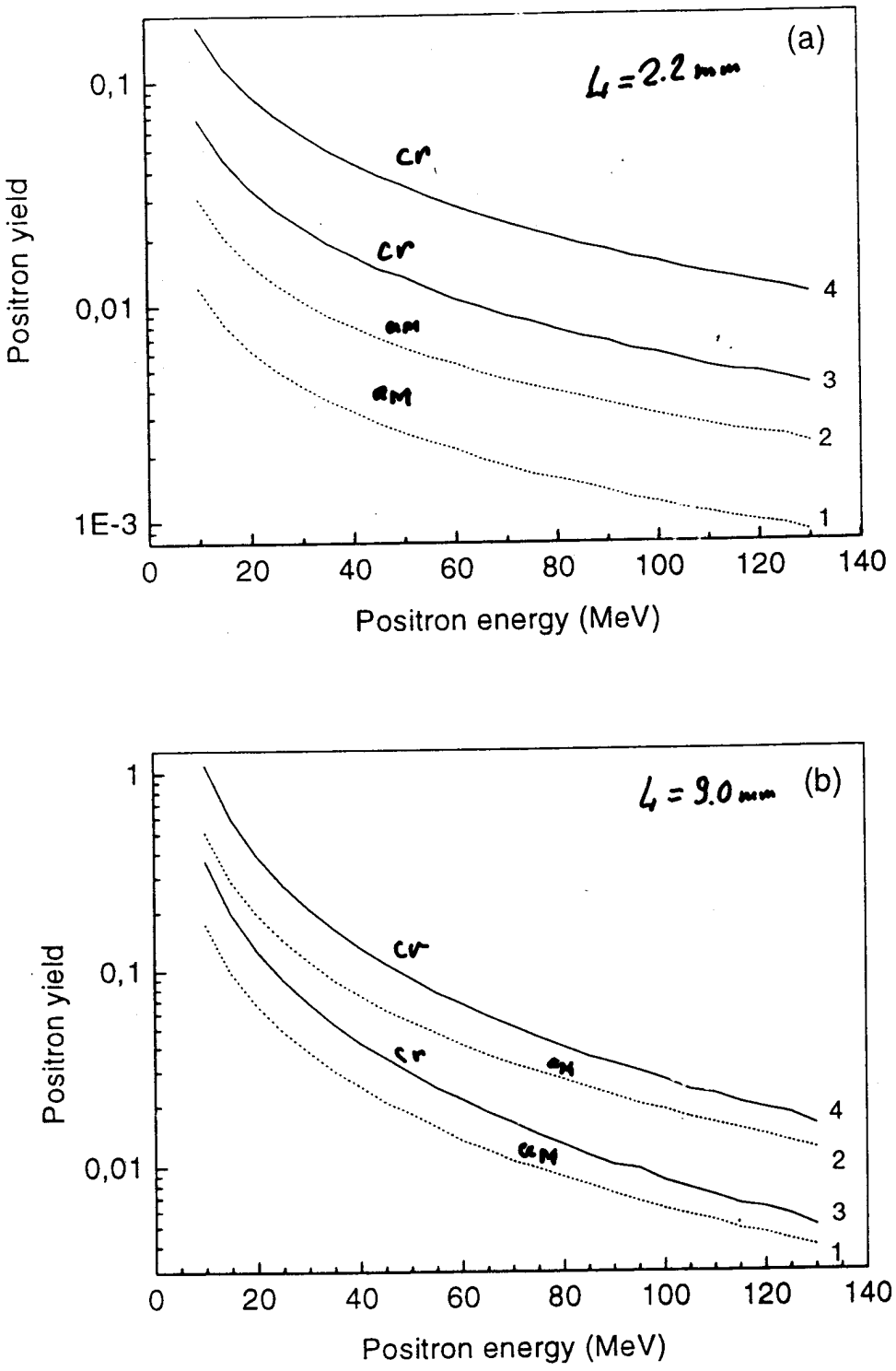

FIG. 4: Positron yield depending on energy at $L = 2.2$ mm (a) and $L = 9.0$ mm (b) for $p_{\perp}^{max} =$ 2.5 MeV/c (curves 1 and 3) and for $p_{\perp}^{max} = 5$ MeV/c (curves 2 and 4). Solid curves represent the yield from crystal and dotted from amorphous targets.

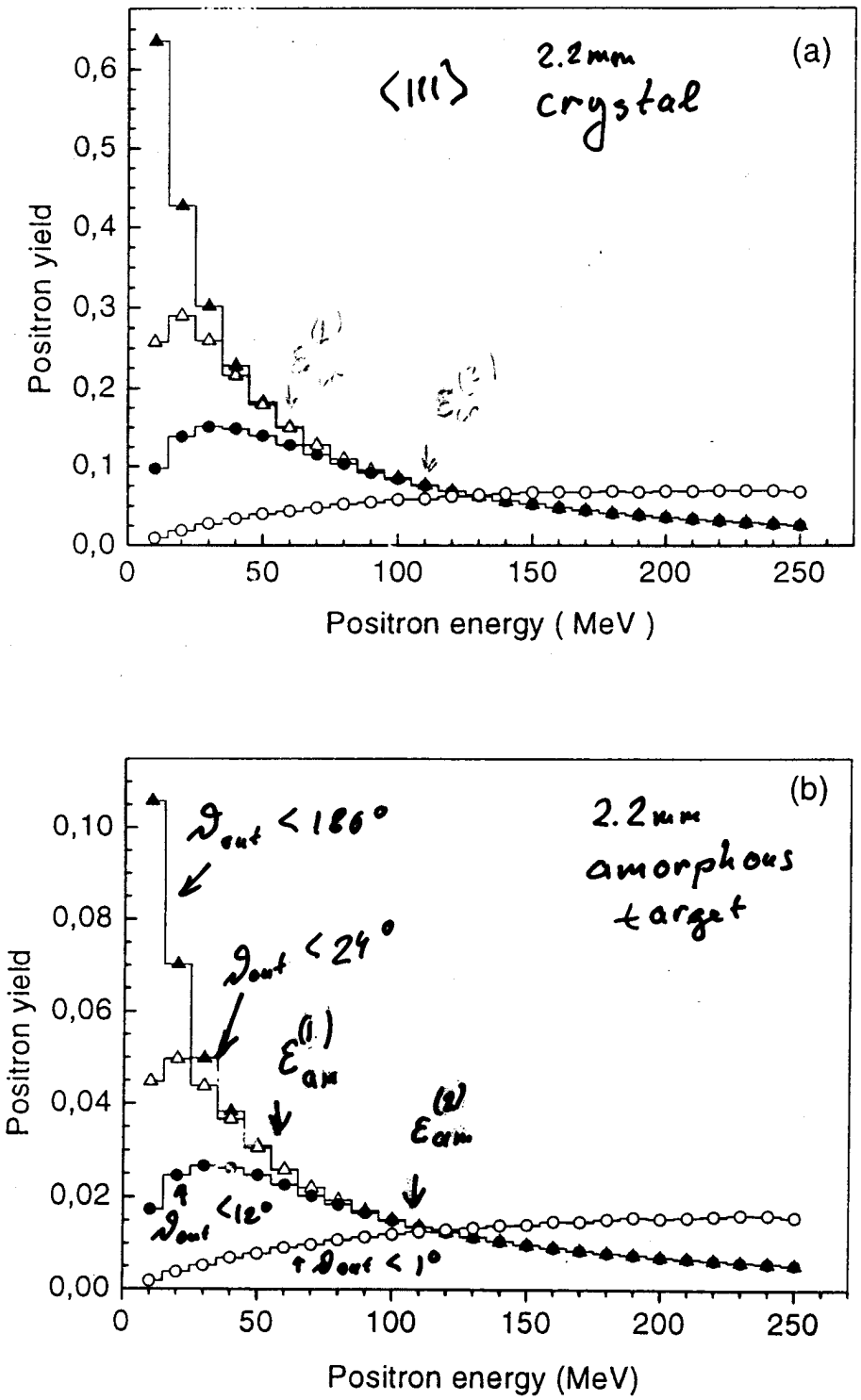

FIG. 2: Positron yield depending on energy from 2.2 - mm - thick crystal (a) and amorphous (b) targets at different collimation . Filled triangles - no collimation ($\vartheta_{out} \leq 180°$), open triangles - $\vartheta_{out} \leq 24°$, filled circles - $\vartheta_{out} \leq 12°$, and open circles - $\vartheta_{out} \leq 1°$ (multiplied by 10).

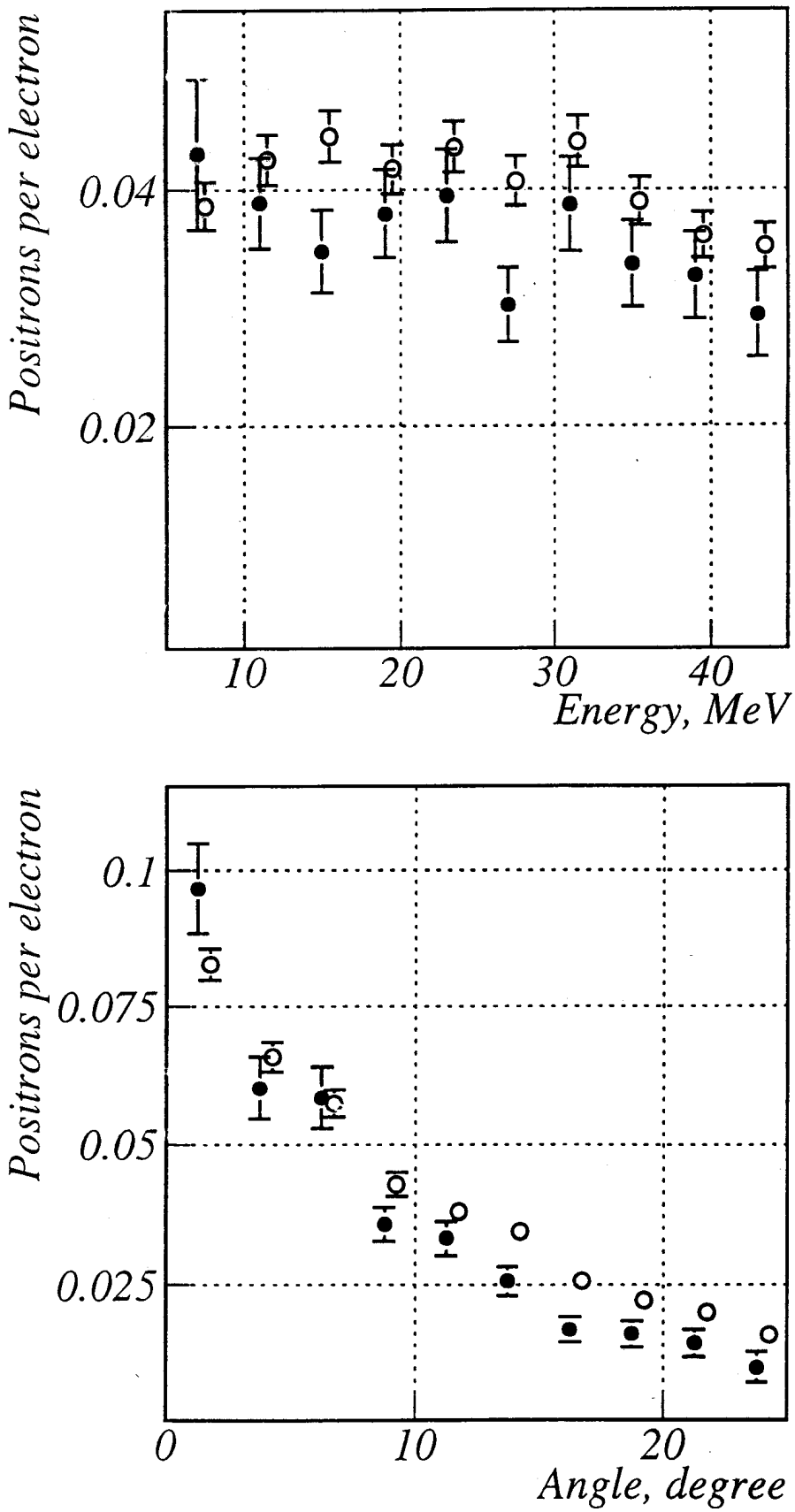

FIG. 1: Spectral (left) and angular (right) distributions of positrons from 10 GeV electrons traversing 8 - mm - thick crystal tungsten target along the < 111 >- axis. Open circles - simulation, filled circles - experiment.

In contrast to the magnitude of the positron yield, the enhancement is not very sensitive to the acceptance conditions. The calculated values of the enhancement(theory) are presented in Table 1 along with those taken from Table 1 of [15] (experiment). Purely statistical errors are figured in Table 1 as theoretical ones. The relative error in PPE was estimated as $N_{ef}^{-1/2}$, where N_{ef} is the mean number of events in the phase space corresponding to the acceptance conditions used in calculations. The total statistics was chosen so that approximately to equalize values of N_{ef} for amorphous and crystal targets of the same thickness. At given total statistics, the quantity N_{ef} increases with growing positron momentum in accord with a shape of the positron spectra at hard collimation shown in Figs. 2,3. This fact leads to a better statistical accuracy for larger momentum. We emphasize that the differences of the estimated and experimental enhancement values are smaller than corresponding experimental errors for all momenta and samples figured in Table 1.

3 Conclusion

Using the simple computer code suggested in [11] and [10], we have compared the theoretical predictions for some characteristics of the electromagnetic shower developing in axially aligned crystals with experimental results reported in [12],[13] and [14],[15]. On the whole, theory and experiment are consistent within the experimental accuracy. From this comparison we also conclude that the accuracy provided by the existing simplified code is at least better than 20%. This accuracy may be slightly improved if we include into consideration some processes like annihilation of positrons or Compton scattering of photons which were ignored as corresponding cross sections are small in the energy region of inter-

lation of the magnitudes of positron production efficiency (PPE), we simply put ϑ_{out}^{max} to 20 mrad. The value of $\Delta p/p$ was chosen to reproduce at applied collimation the experimental magnitude of PPE for the 9.0 - mm - thick amorphous target. Acting in this way, we have got $\Delta p/p = 3.2$ %. We realize that our regard for the acceptance conditions is rather rough. An additional inaccuracy was introduced when we determined the PPE numbers from Fig.5 of [15]. Note that the experimental numbers obtained in a such way, which are presented by filled symbols in Fig.6, do not reproduce exactly the whole set of mean experimental values for the enhancement given in Table 1 of [15]. Moreover, in Fig.5 of [15] there are no experimental points for 2.2 and 5.3 - mm - thick amorphous targets. For these two cases, we present in Fig.6 the values of PPE given by smooth - curve fits corresponding to simulation fitting in Fig.5 of [15]. Bearing all this in mind, we, nevertheless, can assert that a rather good agreement is seen in Fig.6 of the experimental results and our estimations. Relative difference of them is better than 13 % everywhere except the values of PPE at $p = 10$ and 15 Mev/c from both thinnest ($L = 2.2$ mm) targets, where the experimental yield is underestimated by 19 % to 42 %. Note that just for this thickness the largest inaccuracy was introduced while determining the PPE numbers from Fig.5 of [15] at $p = 10$ and 15 Mev/c, as the magnitude of the yield is especially small in this case.

Table 1: Enhancement of the positron yield from crystal targets

Momentum (MeV/c)	Enhancement (2.2-mm-thick)		Enhancement (5.3-mm-thick)		Enhancement (9.0-mm-thick)	
	theory	experiment	theory	experiment	theory	experiment
10	6.0 ± 0.5	6.5 ± 0.6	3.2 ± 0.3	3.4 ± 0.7	2.1 ± 0.2	2.3 ± 0.4
15	5.5 ± 0.3	6.2 ± 0.8	3.2 ± 0.2	3.2 ± 0.5	2.0 ± 0.1	2.0 ± 0.2
20	5.4 ± 0.2	5.1 ± 0.5	2.9 ± 0.1	3.0 ± 0.5	1.8 ± 0.1	1.8 ± 0.2

at $L = 9.0$ mm. These factors turn out to be practically (within an accuracy of a few percent) independent of the total positron momentum p. This fact can be easily understood if we assume that the width of the angular distribution of positrons is completely due to multiple scattering being, thereby, proportional to p^{-1}. Such assumption is confirmed by results of the calculation shown in Fig.5 for two groups of positrons. One of them contains positrons having momentum in the interval $p \in (8.5 \div 11.5)$ Mev/c , for another group $p \in (17 \div 23)$ Mev/c.

For the given target, the width of the angular distribution of positrons with $p \approx 10$ Mev/c is approximately twice as much that for $p \approx 20$ Mev/c as expected. The width of every distribution evidently increases when we go on to the thicker target of the same kind. Comparing angular distributions from crystal and amorphous targets of the same thickness, we find that at $L = 9.0$ mm the distributions are somewhat (about 1.5°) wider in the crystal case for both groups. In units of FWHM of the distribution from the crystal target these differences are about 6.5 % at $p \approx 10$ Mev/c and 14 % at $p \approx 20$ Mev/c. At $L = 2.2$ mm the distribution from the crystal target is wider by 15.5 % at $p \approx 20$ Mev/c whereas this is narrower by 10 % at $p \approx 10$ Mev/c.

Going on to the comparison of our results with those obtained in [15], let us remind that to perform an accurate comparison of such kind, exact information is needed concerning the acceptance conditions and registration efficiency of detectors in the experiment. As noted in [15], at $p = 20$ Mev/c, the momentum acceptance $(\Delta p/p)$ was 3 % (FWHM) and the polar angle acceptance was less than 20 mrad (FWHM). Since the shape of the acceptance curves was unavailable to us, we have tried to simulate experimental conditions using the same angular collimation $\vartheta_{out} \leq \vartheta_{out}^{max}$ and the same value of $\Delta p/p$ for all momenta and targets. So, at the calcu-

the yield is increased by $6 \div 7$ times for a crystal and by $17 \div 20$ times for amorphous samples. As a result, the enhancement at $L = 9.0$ mm is almost 3 times less than at $L = 2.2$ mm in this energy range. At $L = 9.0$ mm the enhancement is peaked in the first bin ($\varepsilon \in (5 \div 15)$ MeV) for every collimation. Its maximum values are $\mu_{max}(\vartheta_{out} \leq 180°) \simeq 2.25$, $\mu_{max}(\vartheta_{out} \leq 24°) \simeq 2.15$, $\mu_{max}(\vartheta_{out} \leq 12°) \simeq 2.08$, and $\mu_{max}(\vartheta_{out} \leq 1°) \simeq 2.06$. The enhancement monotonically decreases with growing positron energy and approximately halves at $\varepsilon \approx 250$ MeV. Thus, positron spectra from the crystal target are softer at $L = 9.0$ mm as well, and this property is much more pronounced in comparison with $L = 2.2$ mm.

Matching systems can be characterized also by the maximum transverse momentum $p_{\perp}^{max}$ of accepted positrons. In this connection, spectra of positrons having $p_{\perp} < p_{\perp}^{max}$ are of undoubted interest. Such spectra at $L = 2.2$ mm (a) and at $L = 9.0$ mm (b) from crystal and amorphous targets are shown in Fig.4. In contrast to the case of the pure angular selection (cf. Figs.2,3 the position of spectral maxima at limited $p_{\perp}$ values is always in the first bin ($\varepsilon \in (7.5 \div 12.5)$ MeV). Corresponding maximum values are $\mu_{max}(5\ MeV/c) \simeq 5.82$, $\mu_{max}(2.5\ MeV/c) \simeq 5.62$ at $L = 2.2$ mm and $\mu_{max}(5\ MeV/c) \simeq 2.17$, $\mu_{max}(2.5\ MeV/c) \simeq 2.11$ at $L = 9.0$ mm. The enhancement monotonically decreases with growing positron energy. Its variation over the whole energy interval presented in Fig.4 is about 15 % at $L = 2.2$ mm and 40 % at $L = 9.0$ mm. So, for this selection too, positron spectra from crystal targets are softer than those from amorphous targets of the same thickness. The interesting feature of spectral curves in Fig.4 is the similarity of those obtained for two different values of $p_{\perp}^{max}$ from the same target. The scaling factors η are $\eta_{cr} \simeq 2.6$, $\eta_{am} \simeq 2.5$ at $L = 2.2$ mm and $\eta_{cr} \simeq 3.1$, $\eta_{am} \simeq 3.0$

The specific features of the radiation under consideration, which occurs for electrons moving in a continuous potential of the axes (planes), are dictated by the particles which are in the channel and are not too high above the barrier. The contribution of these particles can be enhanced by a photon collimator. For this purpose, the collimation angle ϑ_{col} (we count it from the axis oriented to the centre of the collimator) should be chosen approximately equal to the Lindhard angle $\vartheta_{col} \approx \vartheta_c$. On the other hand, if $\vartheta_{col} < m/\varepsilon \equiv 1/\gamma$, we shall omit a fraction of the radiation of interest. For energies from several hundreds of MeV to several GeV considered, we have $\vartheta_s \gg 1/\gamma$ and $\vartheta_s \gg \vartheta_c$ at a crystal thickness $L \approx L_0$. Thus, the condition

$$\max\left(\frac{1}{\gamma}, \vartheta_c\right) \lesssim \vartheta_{col} \ll \vartheta_s \tag{4}$$

assumed to be satisfied and then the factor $\exp\left(-r_\perp^2/g(l)\right)$ can be substituted for unity[3]) for particles whose radiation reaches the collimator, and the distribution proves to be uniform in a transverse phase space. As a consequence, for the intensity of the radiation under consideration (labelled by "ch") at the depth l we have

$$\frac{dI_{ch}}{d\Omega} = \frac{\bar{I}}{\pi g(l)}, \tag{5}$$

where $\bar{I} = \int I(x)\,dx/d_{pl}$ for the plane and $\bar{I} = \int I(\varrho)\,d^2\varrho/S$ for the axis. It is worth noting that $\bar{I}$ coincides with I_{as}, the asymptotic value achieved by the intensity at the incident angles $\vartheta_0 \geqq \vartheta_c$ and $\vartheta_0 \gg \vartheta_c$ for the axial and planar cases, respectively. Emphasize that (5) incorporates the radiation from all the particles rather than from the above-barrier ones only. The appearance of I_{as} in (5) is due to the uniformity of the distribution in transverse phase space under the indicated assumptions, see (4), while the uniformity of the distribution with respect to $v_\perp$ resulted, in (5), in a uniform distribution with respect to the solid angle of emitted photons for the angles $\vartheta_{ph} \lesssim \vartheta_s$.

The values of $\bar{I} = I_{as}$ are readily calculated for any potential of the axes, or planes. For the potentials used, an explicit expression for I_{as} is given by formulae (29) in [1, 2]. Thus, the axial potential has been taken in the form (see [5, 6])

$$U(x) = V_0\left[\ln\left(1 + \frac{1}{x + \beta}\right) - \ln\left(1 + \frac{1}{x_0 + \beta}\right)\right]. \tag{6}$$

For it,

$$\bar{I} = I_{as} = I_0 \varphi(\beta), \tag{7}$$

where

$$I_0 = \frac{8\pi e^2 V_0^2 \varepsilon^2}{3m^4} n_\perp, \qquad \varphi(\beta) = (1 + 2\beta)\ln\left(1 + \frac{1}{\beta}\right) - 2. \tag{8}$$

In (6), $x = \varrho^2/a_s^2$ where a_s is the screening radius and the parameter β is proportional to the squared amplitude of thermal vibrations. In [6, 1] we took $V_0 = Ze^2/d$ where d is the average distance between the atoms in the chain, and the parameters β and a_s were determined by means of the fitting procedure described in [6]. Their values for the $\langle 100\rangle$ axis of some substances are listed in the tables of [6, 1]. For the $\langle 111\rangle$ axis, we have made a three-parametric fitting: the quantity V_0 is regarded to be a fitting parameter as well. The results of this procedure are illustrated in Table 1.

$\vartheta_{out} \leq 24°$ are overlapping within precision better than 1 % starting from $\varepsilon_{cr}^{(1)} \simeq 55$ MeV. In turn, from $\varepsilon_{cr}^{(2)} \simeq 110$ MeV, the same happens with curves corresponding to $\vartheta_{out} \leq 24°$ and $\vartheta_{out} \leq 12°$. Such behavior is also seen in Fig.2 (b) for the amorphous target where $\varepsilon_{am}^{(1)} \simeq 50$ MeV and $\varepsilon_{am}^{(2)} \simeq 105$ MeV. In other words, positrons with energies $\varepsilon > \varepsilon^{(1)}$ are practically concentrated within the cone $\vartheta_{out} \leq 24°$ and those with $\varepsilon > \varepsilon^{(2)}$ have $\vartheta_{out} \leq 12°$. In accordance with this picture, the spectral maximum is shifted to the right while the width of the distribution increases when the collimation angle decreases. The enhancement μ, being bin-by-bin ratio of the positron yield from the crystal target to that from the amorphous one at the same collimation, is almost constant for $\varepsilon <$ 45 MeV and monotonically decreases with growing positron energy. This means that positron spectra from the crystal target are softer. Somewhat lower values of $\varepsilon^{(1)}, \varepsilon^{(2)}$ in the amorphous case point at the same feature. For given collimation, the variation of the enhancement is about 20 % over the whole energy interval presented in Fig.2. The maximum values of the enhancement at different collimation are $\mu_{max}(\vartheta_{out} \leq 180°) \simeq 6.09$, $\mu_{max}(\vartheta_{out} \leq 24°) \simeq 5.92$, $\mu_{max}(\vartheta_{out} \leq 12°) \simeq 5.67$, and $\mu_{max}(\vartheta_{out} \leq 1°) \simeq 5.29$. Apparently, they diminish as the collimation angle does so. Shown in Fig.3 is the same as in Fig.2 but for the target thickness $L =$ 9.0 mm. The yield at $\vartheta_{out} \leq 1°$ (open circles) is multiplied now by 30. The qualitative behavior of spectra depending on the collimation angle at $L = 9.0$ mm is the same as at $L = 2.2$ mm. However, all the spectra become softer for the larger target thickness. This is indicated already by the increase in $\varepsilon^{(1)}$, $\varepsilon^{(2)}$ values which are now $\varepsilon_{cr}^{(1)} \simeq 85$ MeV, $\varepsilon_{cr}^{(2)} \simeq 185$ MeV, $\varepsilon_{am}^{(1)} \simeq 75$ MeV, $\varepsilon_{am}^{(2)} \simeq 165$ MeV. It is clear that the magnitude of the yield from the thicker target is essentially larger but this increase is different in the crystal and amorphous cases. For example, in the energy range $\varepsilon < 45$ MeV

(ε_{dep}^{am}) in the amorphous one. Such interrelation of ε_{dep}^{cr} and ε_{dep}^{am} should take place in the case of [14], where the crystal thickness is about 1.8 L_{ef} (see discussion in the Introduction). This is confirmed by our calculations which give $\varepsilon_{dep}^{cr} \simeq 11$ MeV and $\varepsilon_{dep}^{am} \simeq 277$ MeV per one incident electron.

2.3 Qualitative features of positron distributions and experiment (KEK) at $\varepsilon_0 = 8$ GeV

In [15] the positron production efficiency from 2.2 - mm, 5.3 - mm and 9.0 - mm - thick tungsten crystals was measured using an 8 - GeV electron beam. Positrons produced in the forward direction with momenta 10, 15 and 20 MeV/c were detected by the magnetic spectrometer. Thus, only several points in the energy distribution were determined under hard collimation conditions. Therefore, before going on to the comparison of the experimental results with our, let us remind some important qualitative features of spectral - angular distributions using 8 GeV electrons and the $< 111 >$ - axis of the tungsten crystals as an example. For the sake of comparison, the corresponding distributions for amorphous tungsten will be presented as well. Below all the quantities characterizing the positron yield are normalized per one incident electron.

The use of matching systems implies some collimation (typically $\vartheta_{out} \leq 25^\circ$) of outgoing positrons. Shown in Fig.2 is the energy dependence (energy step is equal to 10 MeV) of the positron yield from crystal (a) and amorphous (b) targets of the same thickness $L = 2.2$ mm. In the case of the hard collimation, when $\vartheta_{out} \leq 1^\circ$ (open circles), the yield is multiplied by 10 to make it visible. The larger the positron energy, the smaller is the typical value of ϑ_{out} since both production and multiple scattering processes are characterized by smaller angles for higher energies. This is seen in Fig.2 (a) where the spectral curves for $\vartheta_{out} < 180^\circ$ and that for

positrons having energies in the 5÷45 MeV range. We emphasize that the relative difference between measured and simulated results typically does not exceed 20 % in both spectral and angular distributions as seen in Fig.1. We are aware that preliminary results for another settings used in the same experiment do not contradict with the estimated scale of the difference between the data and theoretical predictions. We hope that this interrelation will not become worse after performing the complete analysis of the data which now is underway. This analysis will also give more detailed information concerning spectral - angular distributions of positrons depending on initial electron energies and target thicknesses.

2.2 Experiment (KEK) at $\varepsilon_0 = 3$ GeV

The main goal of the experiment [14] was an attempt to apply the crystal target to the working electron/positron linac, the injector for the electron - positron collider B - Factory at KEK. Thus, the acceptance conditions for created positrons were determined by the momentum acceptance of the positron linac with the matching section which is 8.2 MeV/c $< p <$ 11.6 MeV/c and $p_\perp <$ 2.4 MeV/c. The hybrid target used consists of 1.7 - mm - thick tungsten crystal followed by 7 - mm - thick amorphous tungsten. The observed positron yield was enhanced by the factor 1.40 when the $< 111 >$ crystal axis was aligned with 3 GeV incident electron beam as compared to the case of the disoriented crystal. Our number for this enhancement is 1.47 being only 5 % larger than the experimental one. Note that in the experiment [14] the crystal and amorphous parts of the hybrid target were separated by the distance of 70 mm. This circumstance, which, in principle, may slightly change the enhancement value, was not taken into account in our calculation. Recollect that the amount of the energy deposited in the crystal part (ε^{cr}_{dep}) of the hybrid target may be much smaller than that

simplified description of the shower development takes into account coherent (induced by the regular motion of particles in the field of crystal axes) and incoherent (like that in an amorphous medium) mechanisms of photon emission and pair production processes. The multiple scattering and the ionization energy loss of electrons and positrons are taken into account neglecting crystal effects. The coherent radiation from channelling and moving not very high above the axis potential barrier particles is described using the semi - phenomenological spectrum suggested in [11]. The corresponding computer code was developed. This allows one to calculate energy, angular, and coordinate distributions of positrons emergent from the crystal or hybrid target and to find an amount of the energy deposition. We think that the investigation of such distributions should be the main object of the experiments having the creation of the crystal assisted positron source as their ultimate aim.

2.1 Experiment (CERN) at $\varepsilon_0 = 10$ GeV

Among experiments cited above, spectral - angular distributions of created positrons were measured only in WA103 experiment at CERN (see [12], [13]) where our code was used in simulations as the event generator. This simulation allowed for the acceptance conditions and the efficiency of the detectors used. Shown in Fig.1 taken from [13] is one example of the measured and simulated distributions of positrons from 10 - GeV electrons aligned with the $< 111 >$- axis of the 8 - mm - thick crystal tungsten.

The angular acceptance conditions in WA103 experiment were approximately $|\vartheta_V^{out}| \leq 1.5°$ for the vertical and $0 \leq \vartheta_H^{out} \leq 25°$ for the horizontal angle of outgoing positron with respect to the initial electron beam direction. We shell see below that the shape of the positron spectrum depends on the degree of collimation. The one-dimensional (over ϑ_H^{out}) angular distribution is presented for

present the scale, let us list some values ω_{max} where this spectrum is maximum: $\omega_{max}(1GeV) \simeq 31$ MeV, $\omega_{max}(4GeV) \simeq 170$ MeV, and $\omega_{max}(8GeV) \simeq 490$ MeV. Note that the width of the spectrum is typically several times larger than ω_{max}. The increase in the number of relatively soft photons turns out to be much more pronounced than that in the total radiation intensity. In the end, just this fact leads to the substantial enhancement of the positron yield from crystal targets.

Recently the positron production in axially aligned single crystals was studied in two series of experiments performed at CERN [12], [13] and KEK [14], [15]. The initial energy of electrons was 3 GeV [14], 6 and 10 GeV [13], 8 GeV [15], and 10 GeV [12]. In all cases the initial electron beam was aligned with the $< 111 >$ - axis of the tungsten crystal that sometimes served as the crystal part of the hybrid target which contained an additional amorphous tungsten target. A noticeable enhancement of the low-energy positron yield was observed in all experiments cited above when the yield from the crystal target was compared with that from the amorphous target of the same thickness. The experimental results and our theoretical estimations presented in the next Section display a rather good agreement with each other.

2 Comparison of theory with experiment

Theoretical results for the conditions of the experiments cited above were obtained using the approach developed in [11] and [10] where various positron and photon distributions as well as deposited energies in different crystals were calculated for the energy range of initial electrons from 2 to 300 GeV. In these papers, all the formulas used in Monte-Carlo simulations of the specific $e^-e^+\gamma$ - shower characteristics are given in the explicit form. Remember that our

ergy region. The substantial advance in the description of shower formation at axial alignment was caused by the invention of the semi - phenomenological radiation spectrum [11] . This allows one to consider the relatively low (of a few GeV) energy range of the initial electrons which is presumed for the efficient positron source. The radiation intensity increases with the initial electron energy. As a result, at some energy the effective radiation length L_{ef} in the crystal becomes smaller than the conventional radiation length L_{rad} and continues its decrease at further increase of the energy. All numerical examples will be given below for the electron beam aligned with the $< 111 >$ - axis of the tungsten crystals. Then we have for the quantity L_{ef} defined as in Sec.3 of [11]: $L_{ef}(1\ \mathrm{Gev}) \simeq 0.166$ cm, $L_{ef}(4\ \mathrm{Gev}) \simeq 0.084$ cm, and $L_{ef}(8\ \mathrm{Gev}) \simeq 0.061$ cm. In the hybrid target which consists of the crystal part followed by the amorphous one, the thickness of the crystal constituent of several L_{ef} is obviously quite enough. Indeed, at the depth $L_0 \approx (3 \div 4)L_{ef}$ most of the particles, including the initial electrons, are sufficiently soft to reduce the coherent contribution to the radiation to the level of the incoherent one. Thereby, the further development of the shower proceeds more or less in the same way for the crystal or amorphous type of the remaining part of the target. We emphasize that the crystal part $L \leq L_0$ of the target serves as the radiator, and secondary charged particles are still not so numerous at this stage of the shower development. Therefore only a small portion of the total energy loss is deposited in the crystal part of the target which considerably reduces a danger of its overheating. The softness of photon spectra is another important feature of the crystal radiator giving additional advantages for the positron production in comparison with the entirely amorphous target. To get more definite idea concerning the shape of the power spectrum one can use its explicit form given by Eq.(2) in [11]. To

[1],the radiation intensity in a crystal exceeds that of the conventional bremsstrahlung starting with electron energies $\varepsilon \sim 1$ GeV. Simple estimations of the width of the power spectrum performed indicate a soft character of this spectrum. So '...a source of hard and directed radiation concentrated within a comparatively narrow frequency range...' was proposed in [1]. Basing on these properties of the photon emission process, the use of this phenomenon in positron source for future accelerators was proposed [2]. The pair production rate which is due to the coherent (crystal) effects exceeds that of the standard (Bethe-Heitler) mechanism starting with photon energies $\omega \simeq \omega_{th}$. The value of ω_{th} is about 22 GeV for the $< 111 >$ - axis of tungsten being several times larger for another crystals. (See review [3] and recent book [4] for further details concerning QED - processes in crystals.) For energies well above ω_{th}, the crystal effects become really strong and may be used to create effective and compact electromagnetic calorimeters [5]. For very high energies ($\varepsilon \gg \omega_{th}$) of initial and created particles, kinetic equations describing the shower development were solved analytically [6]. Though the initial electron energies were high enough in the first experimental investigation [7] of shower formation in crystals, energies of detected particles were too low to allow us the direct comparison with [6]. To explain the results of [7], Monte-Carlo simulations were performed in [8]. The probabilities of basic processes used in [8] were obtained within so-called constant field approximation. A good agreement was demonstrated in [8] with the results of [7] for Ge crystals.

When the initial electron energy is below ω_{th}, photons are mainly emitted with energies $\omega \ll \omega_{th}$ and so, up to minor modifications (see [9], [10]), the pair production process proceeds in a crystal as in an amorphous medium. The enhancement of radiation from initial electrons is thereby the main crystal effect in this en-

Comparison of theory with experiment for positron production from high-energy electrons moving along crystal axes

B. S.
Phys. Rev ST Accel. Beams, 5, 121001 (2002)

1 Introduction

An efficient positron source is one of the important components of future electron - positron colliders. Positrons are generated from electrons in the course of the $e^-e^+\gamma$ - shower developing in a medium. In high-energy region, the basic processes involved in the shower development are typically considerably enhanced in oriented crystals as compared with corresponding amorphous media . The most pronounced effects take place at axial alignment when initial electrons are moving along the main axes of a crystal. This alignment alone will be considered below. According to

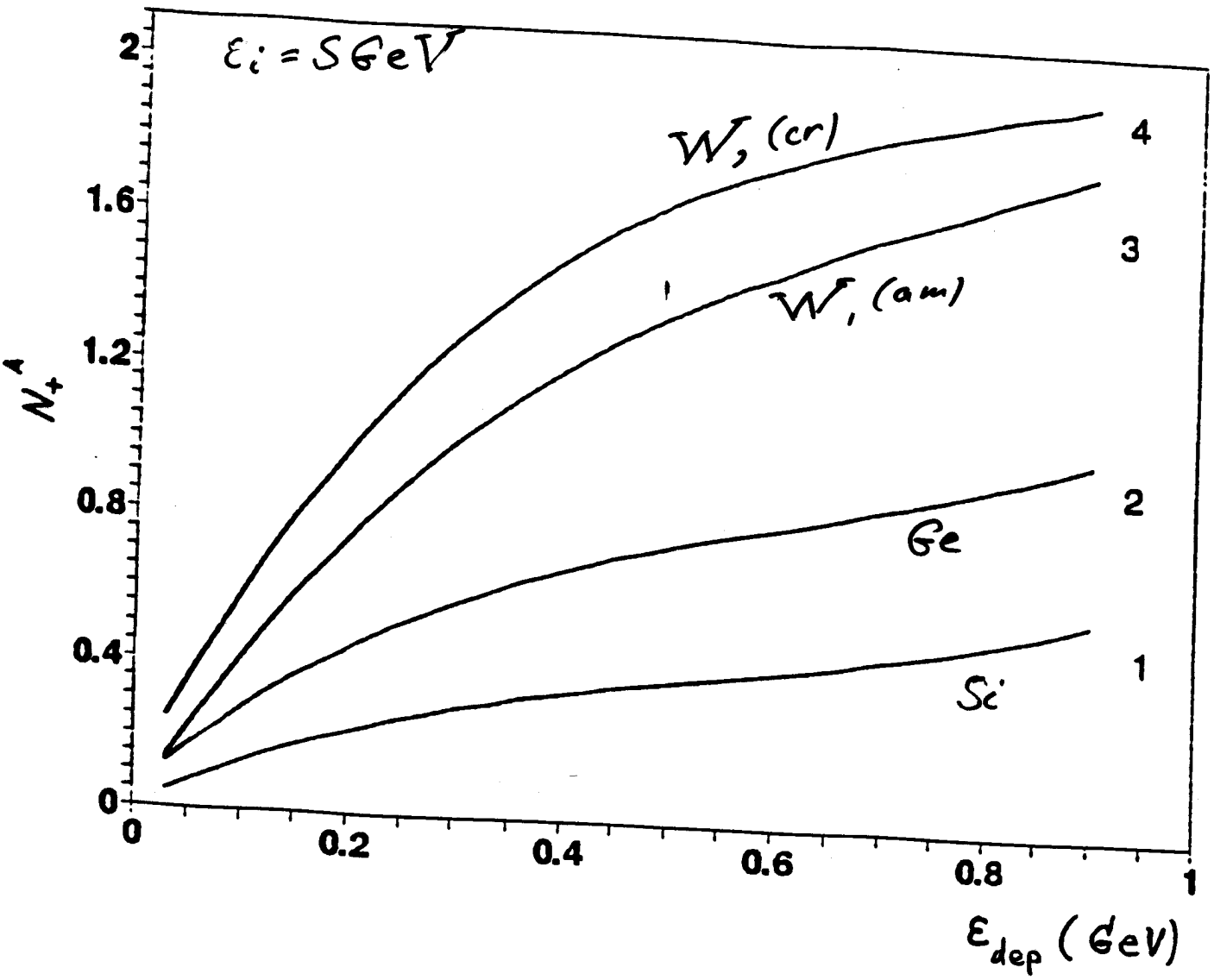
$\varepsilon_i = 5\,GeV$
W, (cr)
W, (am)
Ge
Si
4
3
2
1
N_+^A
0
0.4
0.8
1.2
1.6
2
0.2
0.6
1
ε_{dep} (GeV)

Fig. 9

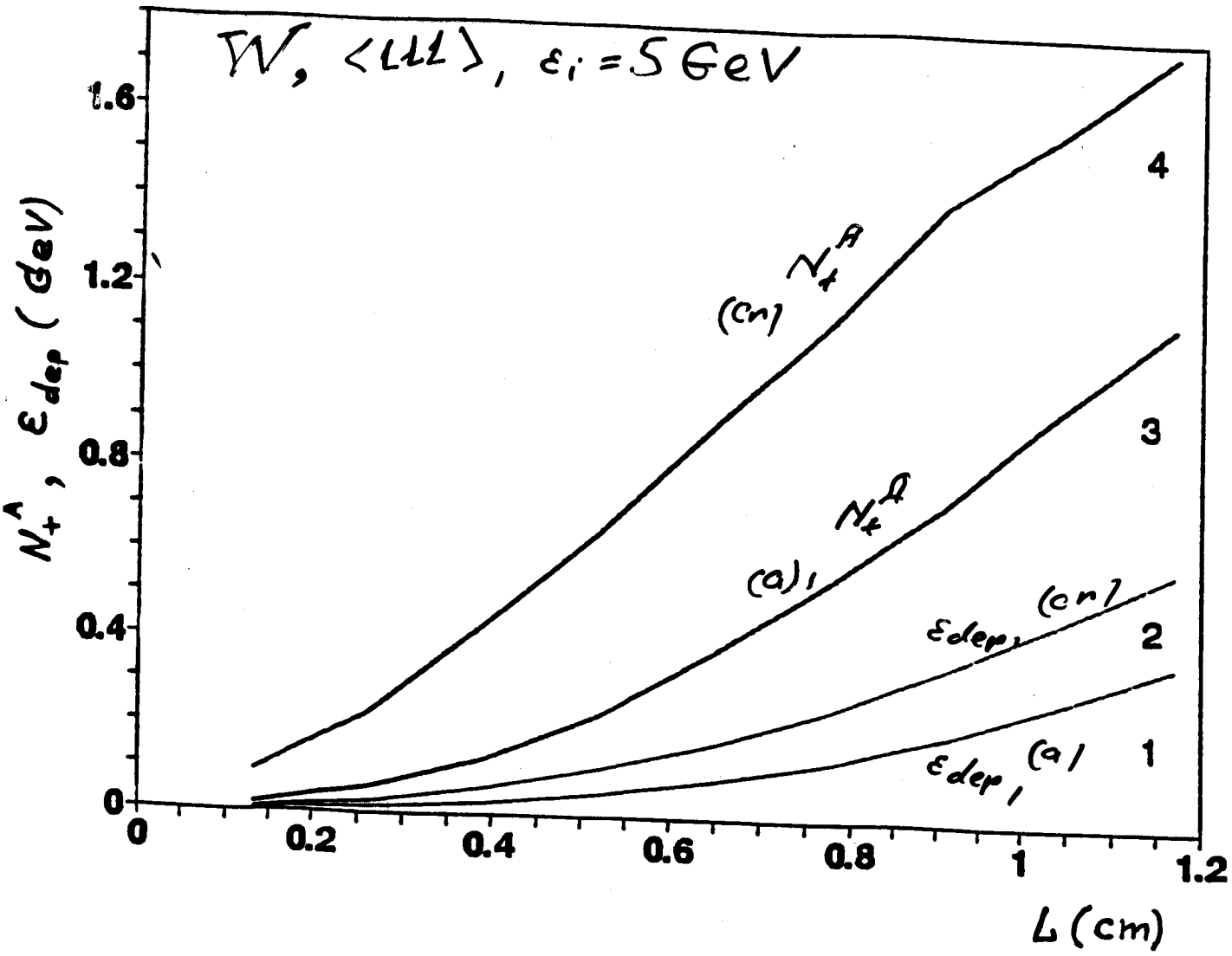
W, <111>, ε_i = 5 GeV
N_+^A , ε_{dep} (GeV)
L (cm)
N_+^A (cm)
N_+^A (a)
ε_{dep} (cm)
ε_{dep} (a)
1
2
3
4
0
0.2
0.4
0.6
0.8
1
1.2
1.6

Fig. 8 (B)

A : accepted $5\,MeV \leq \varepsilon_+ \leq 25\,MeV$

$p_\perp \leq 4\,MeV/c$

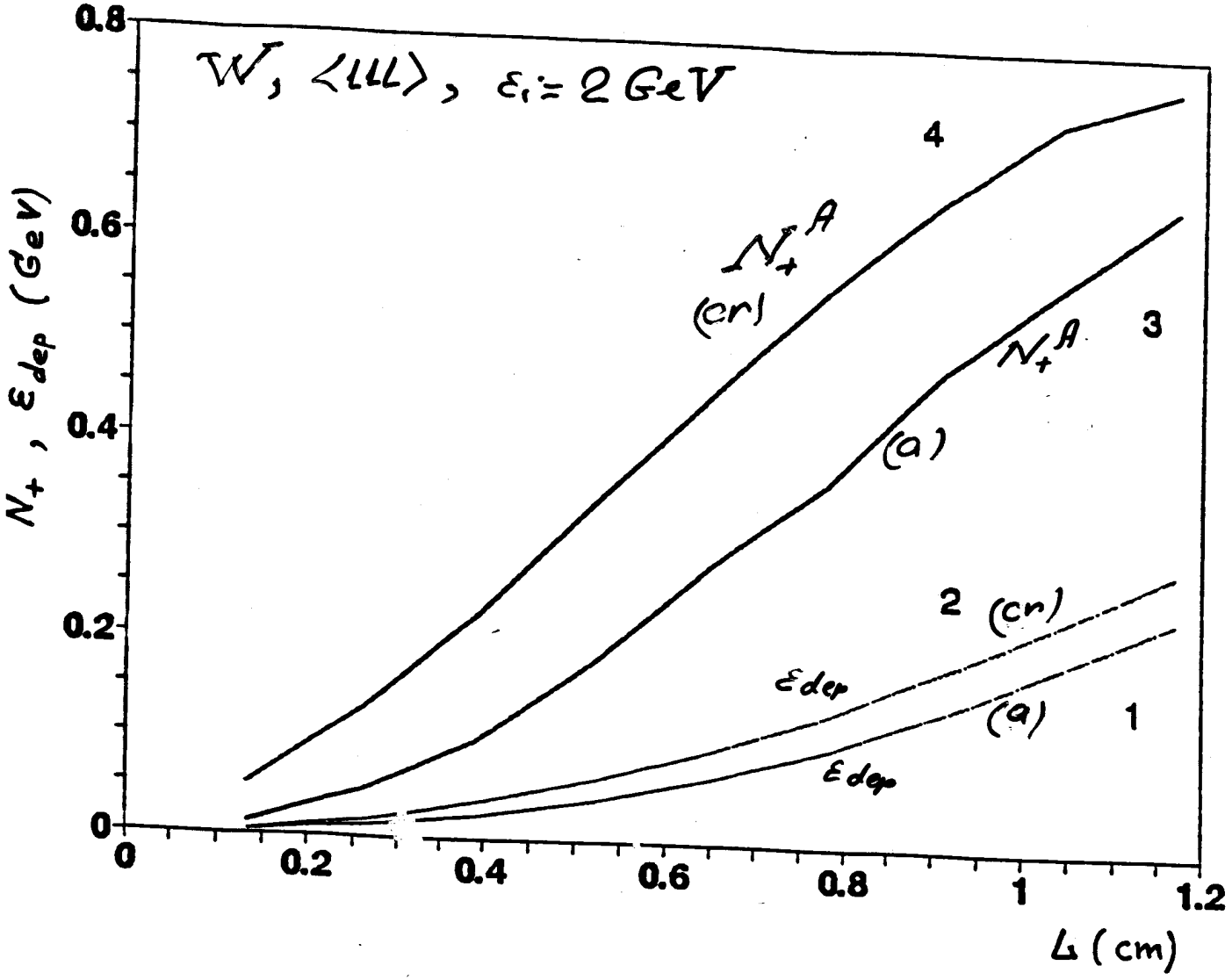

Fig. 8 (a)

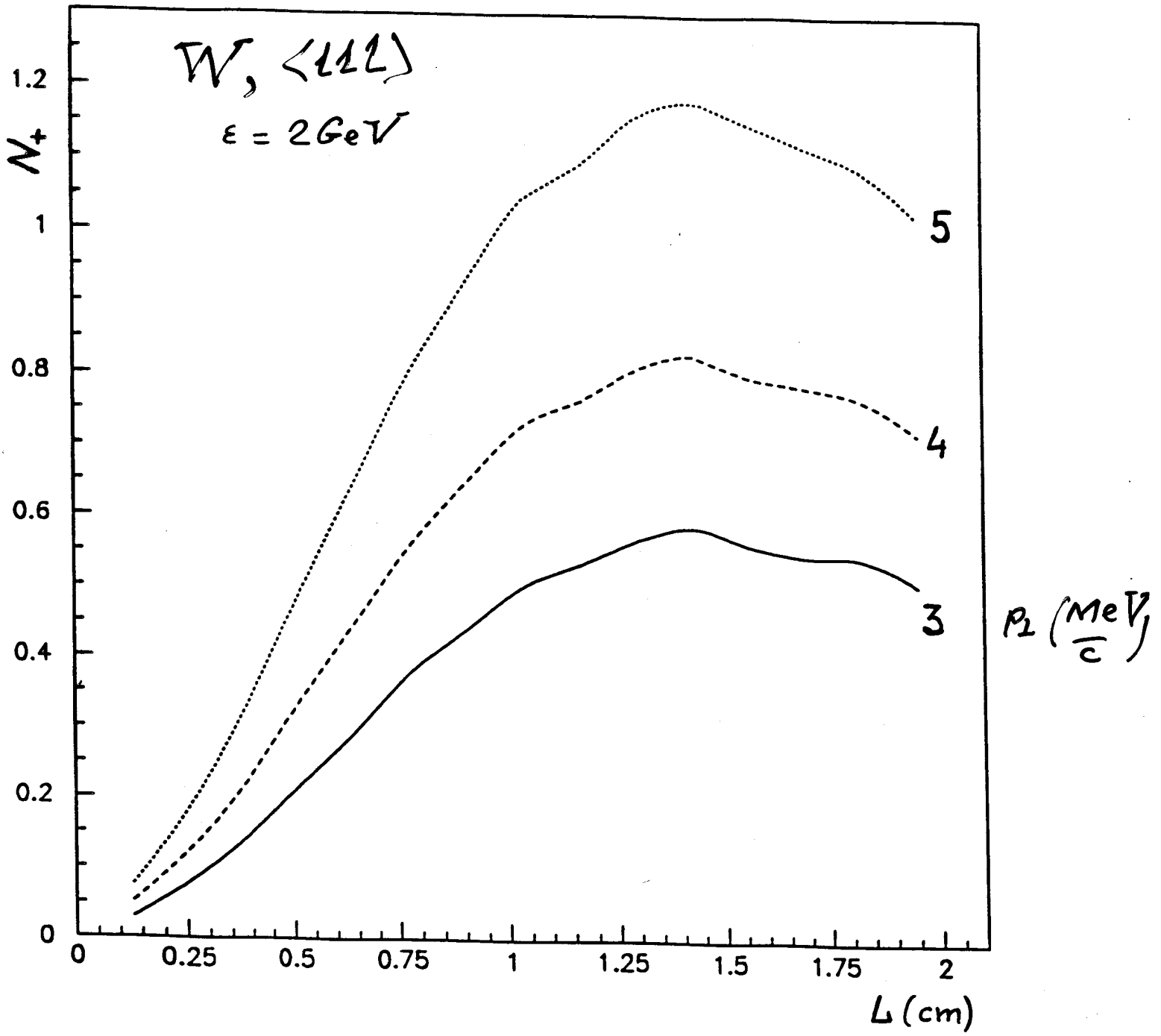
W, <111>
ε = 2GeV
N+
1.2
1
0.8
0.6
0.4
0.2
0
0
0.25
0.5
0.75
1
1.25
1.5
1.75
2
L (cm)
5
4
3
P⊥ (MeV/c)

Fig. 7

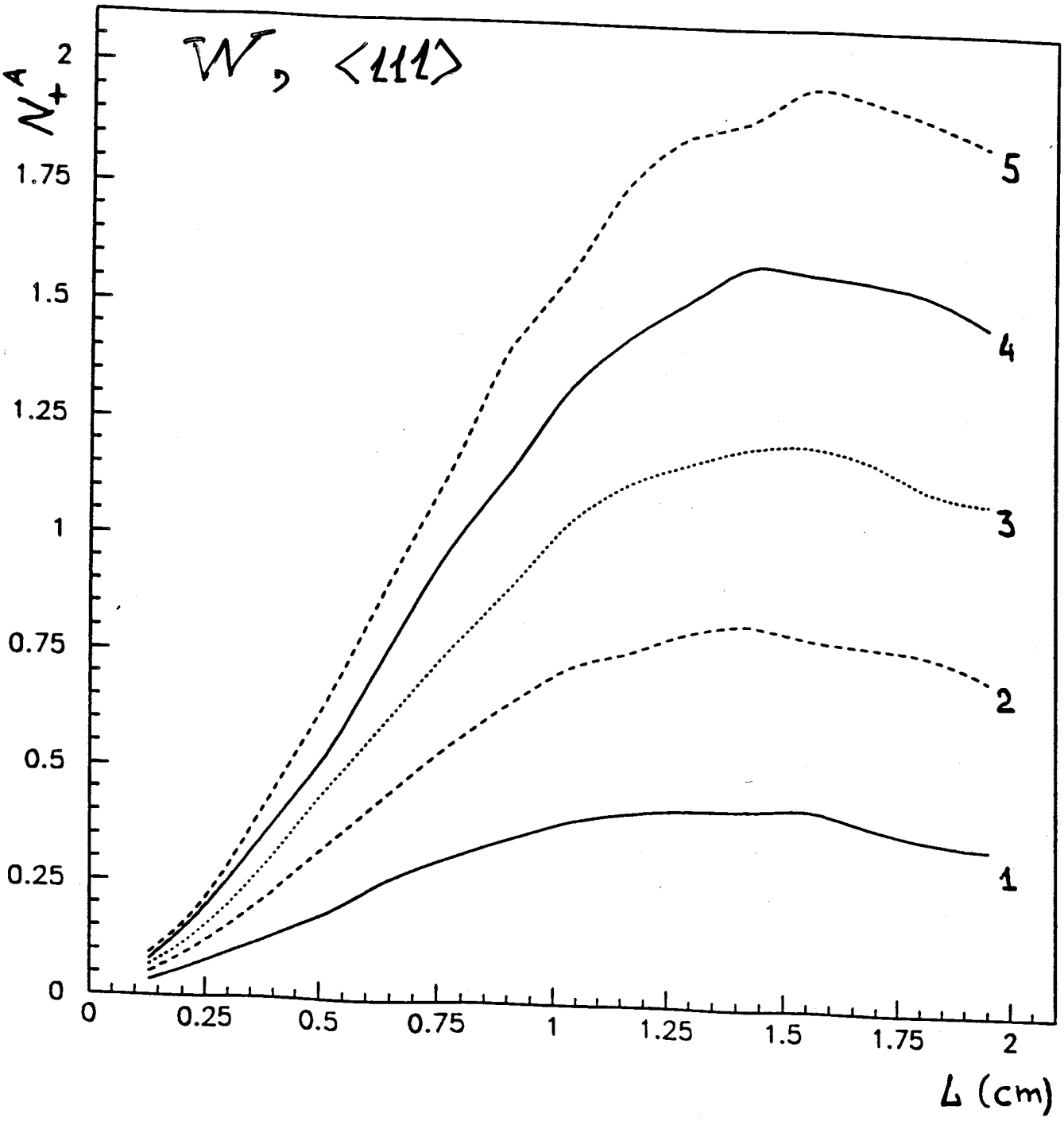
W, <111>
N_+^A
2
1.75
1.5
1.25
1
0.75
0.5
0.25
0
0
0.25
0.5
0.75
1
1.25
1.5
1.75
2
L (cm)
1
2
3
4
5

Fig. 6

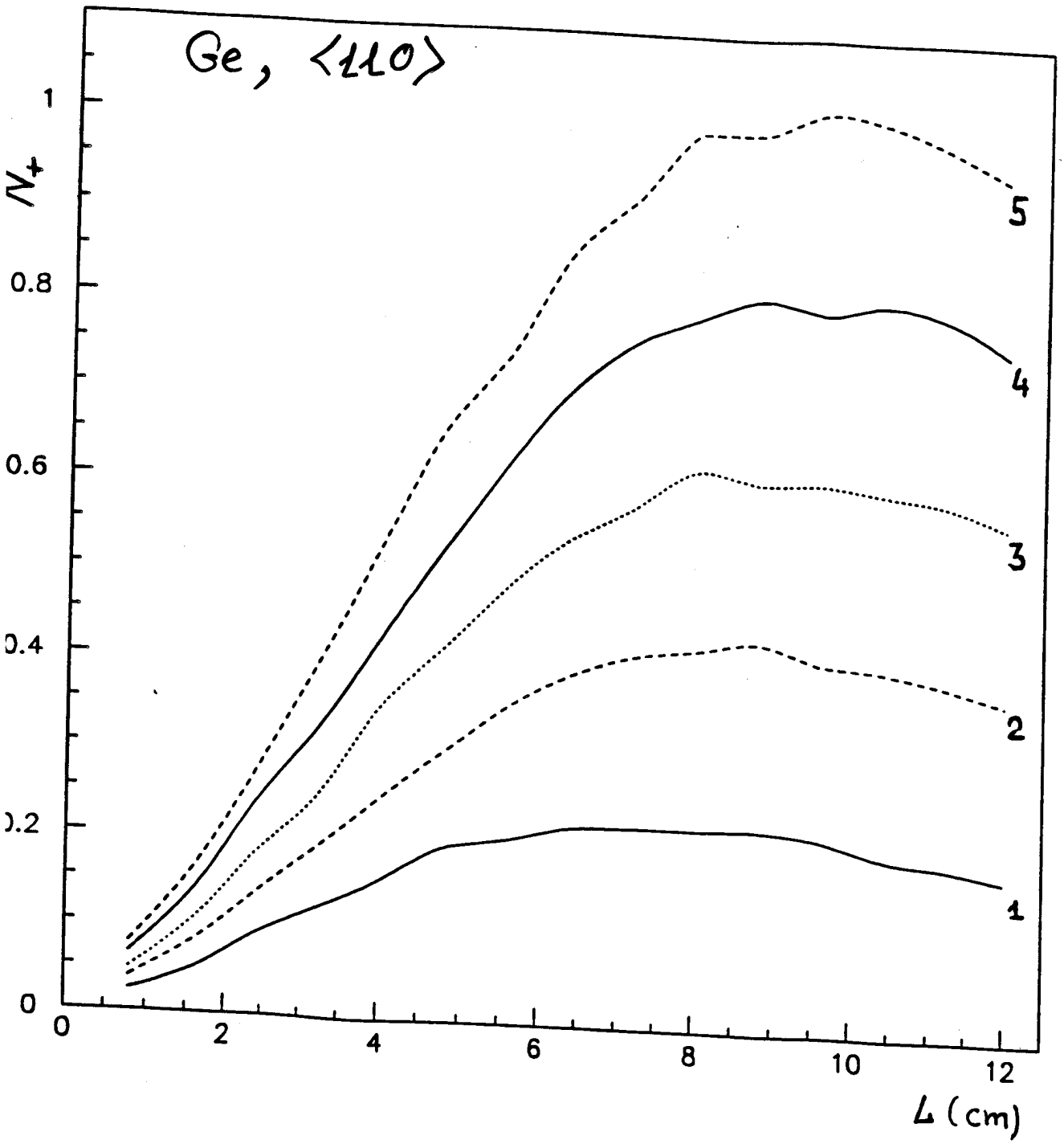

Fig. 5

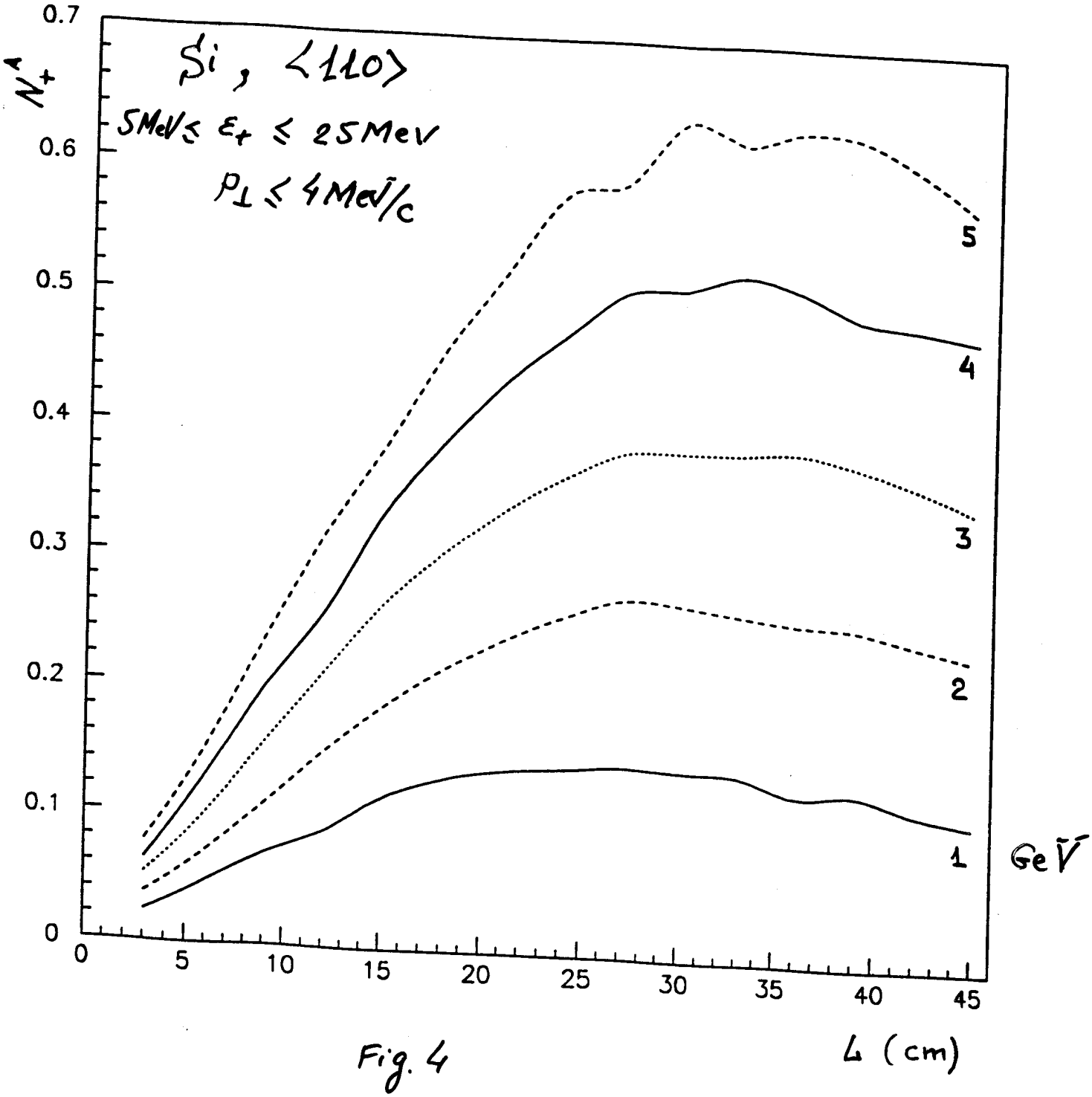
Si , <110>
5MeV ≤ ε+ ≤ 25MeV
p⊥ ≤ 4MeV/c
N+
0.7
0.6
0.5
0.4
0.3
0.2
0.1
0
0
5
10
15
20
25
30
35
40
45
1
2
3
4
5
GeV
L (cm)

Fig. 4

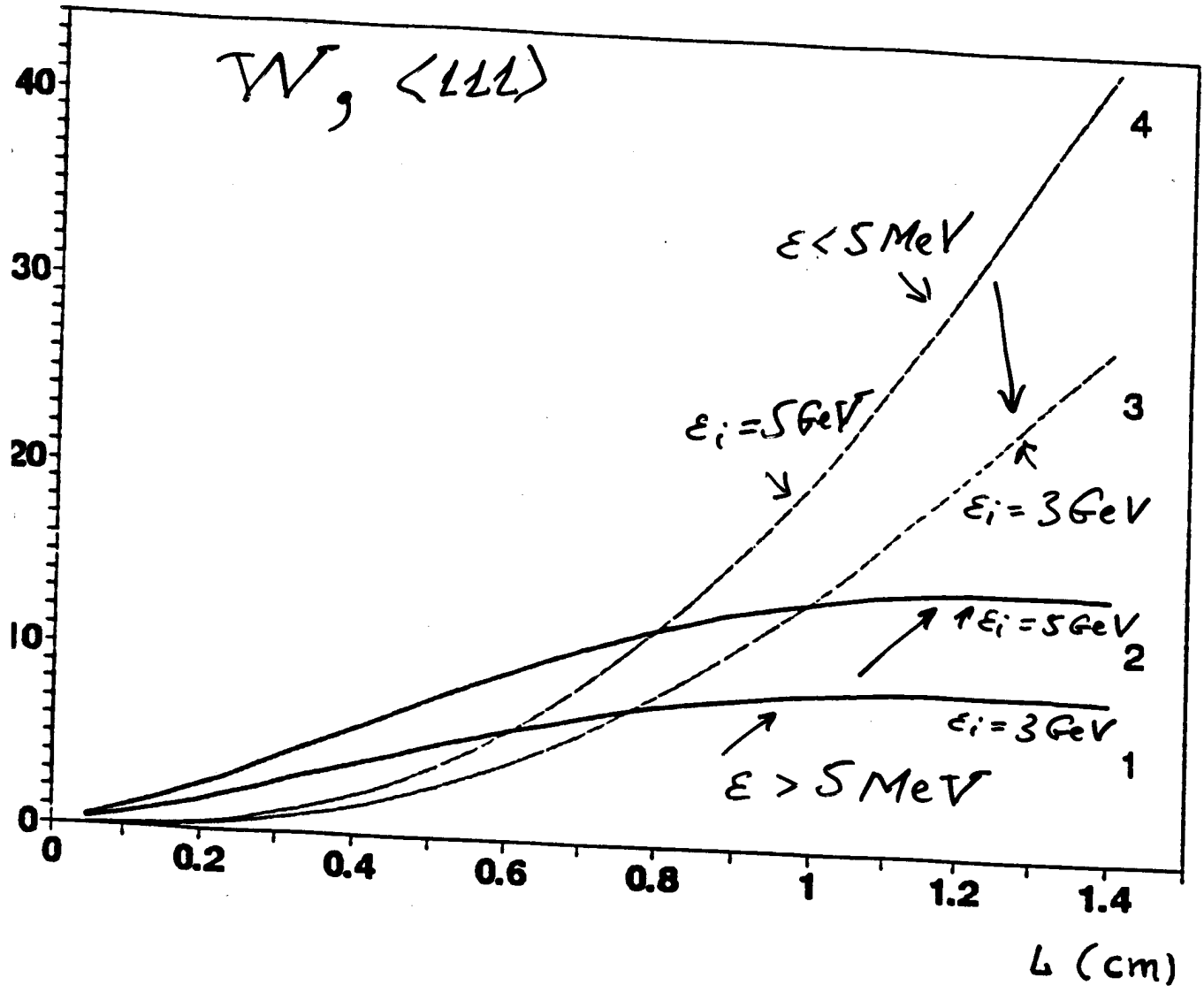
W, <L12>
40
30
20
10
0
0
0.2
0.4
0.6
0.8
1
1.2
1.4
L (cm)
ε<5MeV
4
εi=5GeV
3
εi=3GeV
εi=5GeV
2
εi=3GeV
ε>5MeV
1

Fig. 3

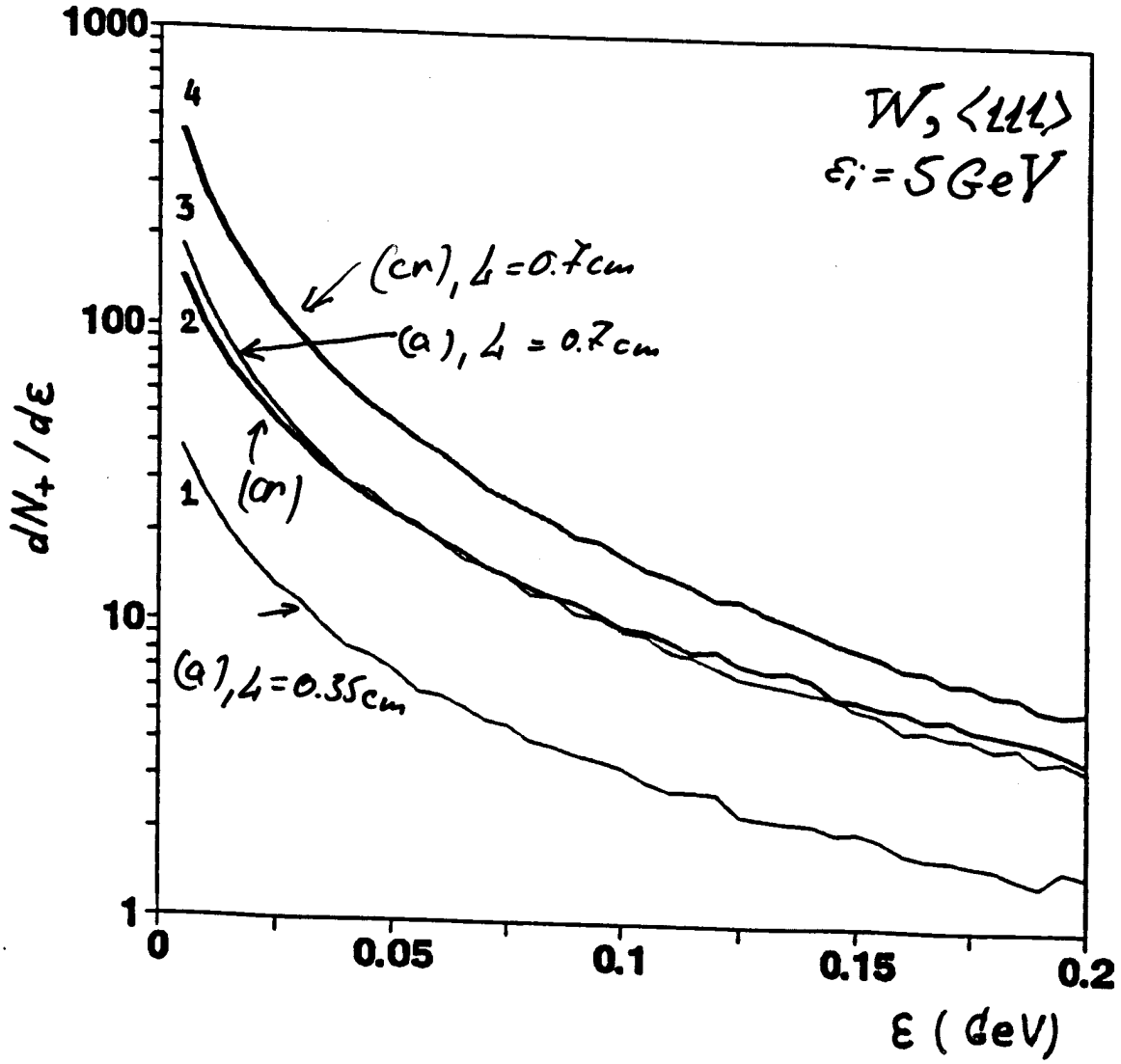
1000
100
10
1
0
0.05
0.1
0.15
0.2
dN+ / dε
ε (keV)
W, <111>
ε_i = 5 keV
(cr), L = 0.7 cm
(a), L = 0.7 cm
(cr)
(a), L = 0.35 cm
1
2
3
4

Fig. 2 (b)

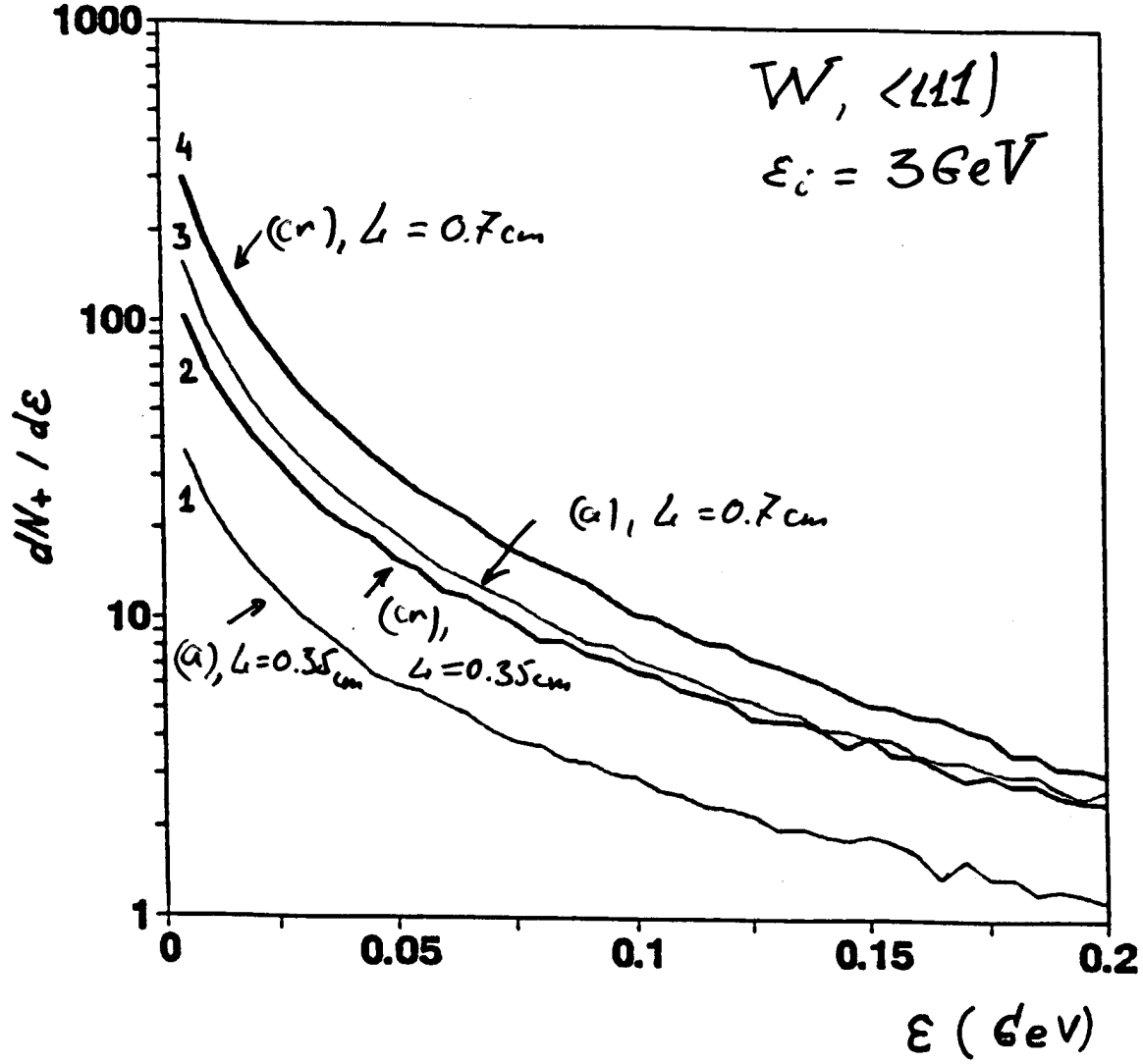
1000
100
10
1
dN+ / dε
W, <111>
εi = 3GeV
4
3
2
1
(cr), L = 0.7cm
(a), L = 0.7cm
(cr), L = 0.35cm
(a), L = 0.35cm
0
0.05
0.1
0.15
0.2
ε (eV)

Fig. 2 (a)

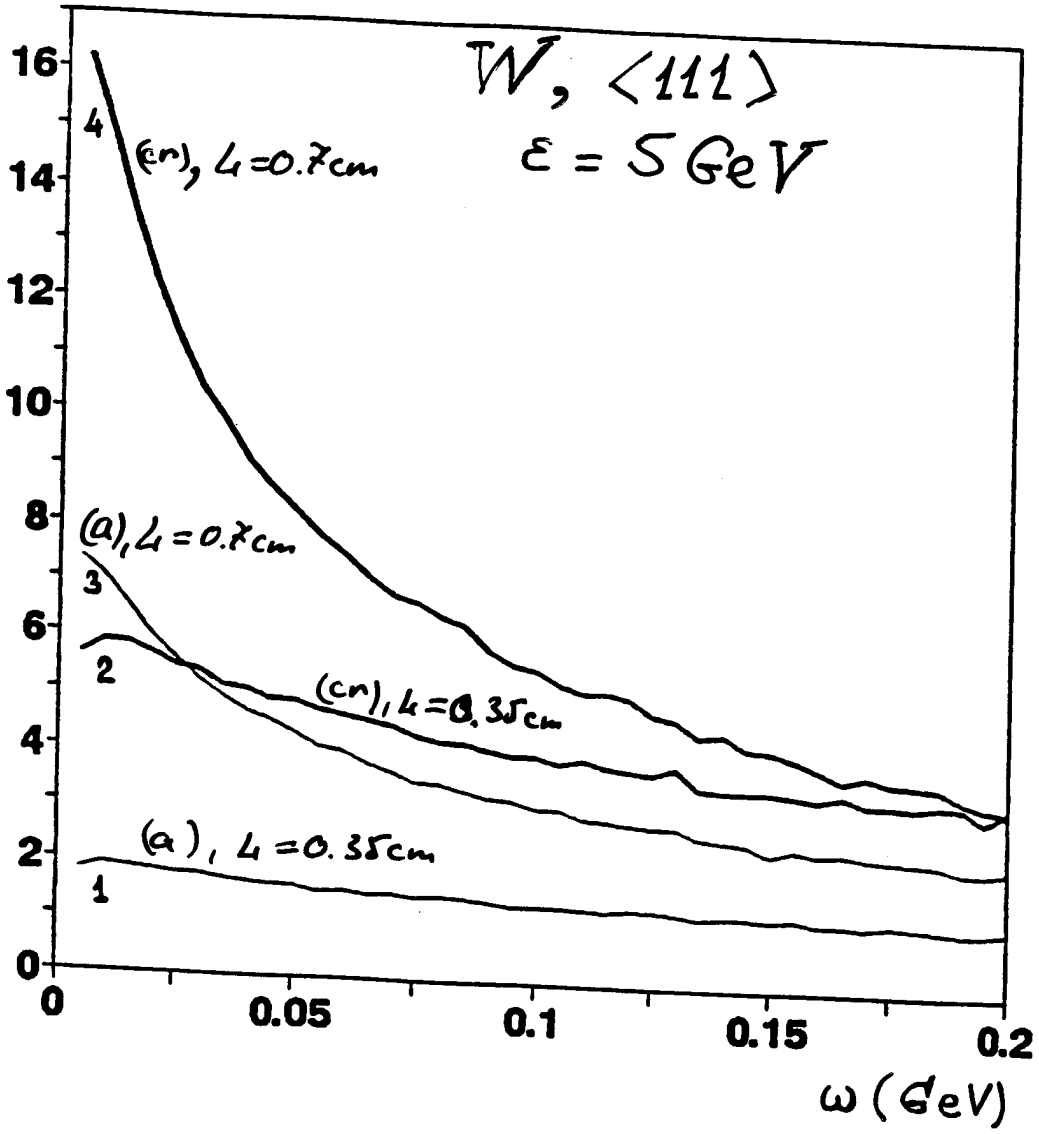
W, <111>
ε = 5 GeV
4
(cr), L=0.7cm
(a), L=0.7cm
3
2
(cr), L=0.35cm
(a), L=0.35cm
1
16
14
12
10
8
6
4
2
0
0
0.05
0.1
0.15
0.2
ω (GeV)

Fig. 1 (B)

1. V.N.Baier, V.M.Katkov,and V.M.Strakhovenko, phys.stat.sol.(b) **133**, 583 (1986). RADIATION YIELD OF HIGH-ENERGY ELECTRONS IN THICK CRYSTAL

2. V.N.Baier, V.M.Katkov,and V.M.Strakhovenko, Sov.Phys.Dokl, **30**, 474 (1986).

3. V.N.Baier, V.M.Katkov,and V.M.Strakhovenko, Nucl. Instr. and Meth. **B 16**, 5 (1986).

4. V.N.Baier, V.M.Katkov,and V.M.Strakhovenko, Nucl. Instr. and Meth. **B 27**, 360 (1987).

5. V.N.Baier, V.M.Katkov,and V.M.Strakhovenko, Sov. Phys.JETP **65**, 686 (1987).

6. V.N.Baier, V.M.Katkov,and V.M.Strakhovenko, phys.stat.sol.(b) **149**, 403 (1988).

7. V.N.Baier, V.M.Katkov,and V.M.Strakhovenko, Sov. Phys.Usp. **32**, 972 (1989).

8. V.N.Baier, V.M.Katkov,and V.M.Strakhovenko, Nucl. Instr. and Meth. **B 103**, 147 (1995). ELECTROMAGNETIC SHOWERS IN CRYSTALS AT GeV ENERGIES

9. V.N.Baier, V.M.Katkov,and V.M.Strakhovenko, Nucl. Instr. and Meth. **B 119**, 131 (1996).

10. V.N.Baier, V.M.Katkov,and V.M.Strakhovenko, *Electromagnetic Processes at High Energies in Oriented Single Crystals*, World Scientific, Sigapore, 1998.

11. V.N.Baier, and V.M.Strakhovenko, Nucl. Instr. and Meth. **B 155**, 403 (1999).

12. V.N.Baier, and V.M.Strakhovenko, Phys.Rev. ST Accel. Beams **5**, 121001 (2002).